Journal of Sound and Vibration (2000) **229**(1), 147–182
Article No. jsvi.1999.2474, available online at http://www.idealibrary.com on IDEAL®

A VELOCITY METHOD FOR ESTIMATING DYNAMIC STRAIN AND STRESS IN PIPES

S. FINNVEDEN†

Department of Vehicle Engineering, KTH SE-100 44 Stockholm, Sweden

AND

R. J. PINNINGTON

Institute of Sound and Vibration Research, University of Southampton, Southampton SO17 1BJ, England

(*Received* 14 *August* 1998, *and in final form* 24 *June* 1999)

A velocity method for estimating dynamic strain and stress in pipe structures is investigated. With this method, predicted or measured spatial average vibration velocity and theoretically derived strain factors are used to estimate maximum strain at the ends of pipes. Theoretical investigation shows that the strain at a point is limited by an expression proportional to the square root of the strain energy density, which in turn is related to its cross-sectional average. For a reverberant field or for an infinite pipe, the average strain energy density is proportional to the mean square velocity. Upon this basis, the non-dimensional strain factor is defined as the maximum strain times the ratio of the sound velocity to the spatial root mean square vibration velocity. Measurements are made confirming that this is a descriptive non-dimensional number. Using a spectral finite element method, numerical experiments are made varying the pipe parameters and considering all 16 homogeneous boundary conditions. While indicating possible limitations of the method when equipment is mounted on pipes, the experiments verify the theoretical results. The velocity method may become useful in engineering practice for assessments of fatigue life.

1. INTRODUCTION

Vibrations in pipes are excited by mechanical machinery, by pumps and by internal turbulent fluid motion. Pipe vibrations cause annoying, sometimes hazardous, noise radiation and can cause failure due to fatigue, possibly resulting in economical and environmental disasters.

Predictions of pipe vibrations are made with the finite element method (FEM) with direct methods formulated in the frequency domain, e.g., references [1–4] and with statistical energy analysis (SEA) [5, 6]. Most of these methods are not yet sufficiently developed to result in commercially available code while the cost, in

† The major part of this work was undertaken while the first author was at the ISVR.

0022-460X/00/010147 + 36 $35.00/0

man and computer time, required for full-scale FE calculation makes this methods application to large pipe structures impractical. Additionally, the lack of knowledge of the sources of vibration makes any prediction doubtful. Therefore, measurements are needed to assess pipe structures integrity, this being increasingly interesting, as there is a demand for "life extension" of existing plants.

In the chemical industry, energy production and on off-shore installations there are often many kilometres of pipes. Clearly, it is impossible to instrument such plants at every point with strain gauges to find maximum strain or stress to predict fatigue life. A more practical cause of action would instead be to measure vibration amplitudes at selected positions using portable accelerometer and analyser equipment.

Previously, relations between vibration velocity and strain have been obtained where the simple outcome is that within an element the strain is approximately proportional to the ratio of the vibration velocity to the dilatational (sound) velocity in the element's material [7–14]. The objective of the present work is to further our understanding of this "velocity method" for estimating strain and in particular its application to pipe structures.

Hunt initiated the method studying single-mode response in rods and beams showing that the maximum strain in a rod (at a vibrational node is equal to the maximum velocity ratio (at an antinode) [7]. Within beams of rectangular cross-section, the maximum strain is a factor of $\sqrt{3}$ larger than the maximum velocity ratio; at a blocked end the maximum strain is increased by an additional 40–65% [7]. Ungar considered wave fields in semi-infinite plate and plate-beam structures deriving the strain as a function of the amplitude of an incoming wave [8]. Ungar defined the "dynamic strain concentration factor" as the ratio of the strain at a restriction (such as a frame) to the average strain within the element. Stearn investigated the statistical variability of the strain within plate and cylinder elements in which there is an approximately diffuse field, showing the variation for frequency band averages to be proportional to the square root of the number of modes within the band [9]. Stearn also calculated and measured the strain concentration at junctions between plate elements with different wall thickness [10]. Norton and Fahy made measurements on an oil-filled pipe verifying, also for such structures, the simple relation between vibrational strain and radial velocity [11]. However, at a restriction in the form of a flange, the measured strain concentration factor was very large, of the order of 10–100. This may be possible as the strain at the flange was compared to the velocity at the same place rather than the vibrations between discontinuities. Koss and Karczub developed a more elaborated version of the velocity method [12]. Accelerometer readings were used to find the amplitudes of the four wave solutions to the beam equations and from this the strain was calculated. Recently, Karczub [13] and Karczub and Norton [14] have reviewed and developed the velocity method for predicting strain.

The present work, as well as the references [7–14], studies perfect structures. Thus, it does not consider geometric strain concentration at imperfections and inhomogeneities; it is restricted to dynamic strain concentration, as defined by Ungar [8].

The dynamic strain concentration is defined by the "transfer function" between average vibration and the maximum principle strain amplitude at pipe ends. Thus, the usefulness of the velocity method is to some extent restricted by the fact that only power spectral data is provided; often fatigue analysis is based on temporal strain information. However, there are methods based on spectral density data, e.g. reference [15], and, in any case, the spectral data provide indication of the severity of vibration. The velocity method is primarily intended to be a screening method.

The present work develops an alternative theoretical approach to the velocity method based on considerations of vibration energy. The maximum strain, and stress, at a point is related to the cross-sectional average of strain energy density. This gives a foundation for arguing that the maximum strain, being related to the strain energy and hence the average kinetic energy, relates to the average vibration velocity in the pipe. This approach differs from that of references [8–10] where the maximum strain is related to the wave amplitude of incoming waves and, to a greater extent, from that of references [7, 14] where the maximum strain is related to the maximum vibration amplitude. It is argued that the energy approach rather than the maximum amplitude approach is conceptually simpler and it relates directly to results from SEA calculations. Moreover, it is easier to estimate average vibration than to find the maximum vibration amplitude.

In section 3, measurements on a pipe structure with a blocked end are presented. The results agree with those by Karczub and Norton [14] apart from a factor $\sqrt{2}$, for which a possible explanation is given. The measurement results are compared to those found with the direct dynamic finite element method presented in reference [4], here developed using routines for calculating average vibration response and strain and stress. The good agreement of the results justifies the numerical approach for simulating vibration velocity and strain.

In section 4, numerical experiments are presented. Dimensional analysis shows that the vibration of pipes is a function of only a few non-dimensional numbers. By varying these and the boundary conditions, 16 in all, a fairly comprehensive investigation is made of the relation between average radial velocity and maximum strain in pipes. The results show the potential for the velocity method for assessing fatigue of pipe structures. However, they also point to a possible limitation for special boundary conditions.

2. MAXIMUM STRAIN AND STRESS IN CYLINDERS

In this section, the stress and strain in cylinders are expressed. Limits for their maxima are found to be proportional to the square root of the strain energy density. For reverberant fields or in wave fields, the strain energy density is related to the average vibration energy. It is argued that the average vibration energy can be estimated by the average radial vibration velocity, which is accessible from comparatively simple measurements.

The motion of the cylinder is described with an implicit time dependence of the form $e^{-i\omega t}$. Thus, the analysis applies for harmonic vibration and stationary random vibration.

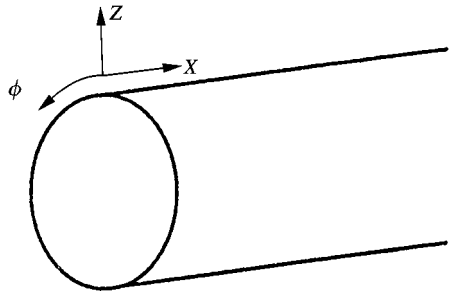

Figure 1. Cylinder co-ordinate system.

2.1. STRAIN AND STRESS IN CYLINDERS

The motion of thin-walled cylinders is investigated using a Fourier decomposition of the circumferential dependence of the displacements and using the Kirchhoff hypothesis [16]. Thus, the strains, in directions specified in Figure 1, are

$$\gamma_{xz} = \gamma_{\phi z} = \gamma_z = 0, \tag{1}$$

while the displacements for trigonometric order n are

$$u_x = (u + z\theta_1)\cos(n\phi), \qquad u_\phi = (v + z\theta_2)\sin(n\phi), \qquad u_z = w\cos(n\phi), \tag{2}$$

where, from equation (1),

$$\theta_1 = -\frac{\partial w}{\partial x}, \qquad \theta_2 = (v + nw)/R. \tag{3}$$

Using the Love–Timoshenko strain–displacement relations for thin-walled cylinders, neglecting all but the dominating terms in the small quantity T_c/R, the remaining three strain components are [17]

$$\gamma_x = (\varepsilon_x + z\kappa_1)\cos(n\phi), \qquad \gamma_\phi = (\varepsilon_\phi + z\kappa_2)\cos(n\phi), \qquad \gamma_{x\phi} = (\gamma + z\tau)\sin(n\phi), \tag{4}$$

where T_c is the cylinder wall thickness and R is the radius and where

$$\varepsilon_x = \frac{\partial u}{\partial x}, \qquad \varepsilon_\phi = \frac{(nv + w)}{R}, \qquad \gamma = -\frac{nu}{R} + \frac{\partial v}{\partial x},$$

$$\kappa_1 = -\frac{\partial^2 w}{\partial x^2}, \qquad \kappa_2 = \frac{nv + n^2 w}{R^2}, \qquad \tau = \frac{2}{R}\left(\frac{\partial v}{\partial x} + n\frac{\partial w}{\partial x}\right). \tag{5}$$

Accordingly, considering an isotropic Hookean material and assuming plane stress [16, p. 14], the stresses are

$$\sigma_x = E'(\gamma_x + v\gamma_\phi), \qquad \sigma_\phi = E'(\gamma_\phi + v\gamma_x), \qquad \sigma_{x\phi} = G\gamma_{x\phi}, \tag{6}$$

where

$$E' = E/(1 - v^2), \qquad G = E/2(1 + v), \tag{7}$$

and where E is Young's modulus and v is Poisson's ratio.

The state of stress at a point is given by the stress tensor, $\mathbf{S}$ [18],

$$\mathbf{S} = \begin{bmatrix} \sigma_x & \sigma_{x\phi} \\ \sigma_{x\phi} & \sigma_\phi \end{bmatrix} = \mathbf{\Phi} * \begin{bmatrix} \sigma_1 & 0 \\ 0 & \sigma_2 \end{bmatrix} * \mathbf{\Phi}^{\mathrm{T}}, \tag{8}$$

where the last equality follows from an eigenvalue decomposition of $\mathbf{S}$. Thus, σ_i are the eigenvalues and the eigenvectors are the columns of $\mathbf{\Phi}$. From this, it follows that if the stress is expressed in the co-ordinate system given by the stress tensor's eigenvectors, the shear stress vanishes and the stresses in these co-ordinates, the principal stresses, are the eigenvalues of $\mathbf{S}$, σ_1 and σ_2. It will be assumed that

$$|\sigma_1| \geqslant |\sigma_2|. \tag{9}$$

Similarly, the strain at a point is given by the strain tensor

$$\mathbf{s} = \begin{bmatrix} \gamma_x & \gamma_{x\phi}/2 \\ \gamma_{x\phi}/2 & \gamma_\phi \end{bmatrix}. \tag{10}$$

For a Hookean material the directions of principal stress and principal strain coincide. Expressed in a co-ordinate system in these directions the shear strain vanishes and the principal strains are γ_1 and γ_2. From equations (6) and (9), for an isotropic material

$$|\gamma_1| \geqslant |\gamma_2|. \tag{11}$$

The maximum stress in a point is σ_1. An upper bound to $|\sigma_1|$ is given by

$$\begin{aligned} |\sigma_1| = E'|\gamma_1 + v\gamma_2| &= E'\sqrt{|\gamma_1|^2 + 2v\mathrm{Re}(\gamma_1^*\gamma_2) + |v\gamma_2|^2} \\ &\leqslant E'\sqrt{|\gamma_1|^2 + 2v\mathrm{Re}(\gamma_1^*\gamma_2) + |\gamma_2|^2} = \sqrt{E'2e_p}, \end{aligned} \tag{12}$$

where γ_1^* denotes the complex conjugate of γ_1 and where e_p is the strain energy density [16, equation (1.85)]. The strain energy density is invariant to co-ordinate transformations, hence it is equally expressed in the cylinder

co-ordinate system

$$e_p = E'/2(\gamma_x\gamma_x^* + v(\gamma_x\gamma_\phi^* + \gamma_\phi\gamma_x^*) + \gamma_\phi\gamma_\phi^* + g\gamma_{x\phi}\gamma_{x\phi}^*), \tag{13}$$

where

$$g = G/E' = (1 - v)/2. \tag{14}$$

To find a similar limit for the maximum principal strain, it is easier to go backwards

$$\begin{aligned} 2e_p/E' &= |\gamma_1 + v\gamma_2|^2 + (1 - v^2)|\gamma_2|^2 \\ &\geqslant (|\gamma_1| - v|\gamma_2|)^2 + (1 - v^2)|\gamma_2|^2 = |\gamma_1|^2(1 - 2v|\gamma_2/\gamma_1| + |\gamma_2/\gamma_1|^2). \end{aligned} \tag{15}$$

This function has a minimum at $|\gamma_2| = v|\gamma_1|$, from which it follows that

$$|\gamma_1| \leqslant \sqrt{\frac{2e_p}{(1 - v^2)E'}} = \sqrt{2e_p/E}, \tag{16}$$

which establishes the limits for the maximum strain and stress. The possible overestimation is found from

$$2e_p/E' \leqslant (|\gamma_1| + v|\gamma_2|)^2 + (1 - v^2)|\gamma_2|^2 = |\gamma_1|^2(1 + 2v|\gamma_2/\gamma_1| + |\gamma_2/\gamma_1|^2). \tag{17}$$

Since by definition $|\gamma_2| \leqslant |\gamma_1|$ this function is maximized for $|\gamma_2| = |\gamma_1|$. Therefore

$$|\gamma_1| \leqslant \sqrt{2e_p/E} \leqslant |\gamma_1|\sqrt{2/(1 - v)}. \tag{18a}$$

By similar calculations

$$|\sigma_1| \leqslant \sqrt{2e_pE'} \leqslant |\sigma_1|\sqrt{2/(1 - v)}. \tag{18b}$$

For an isotropic material $0 \leqslant v \leqslant 0{\cdot}5$. Equations (18) indicate that the maximum overestimation of a factor of two occurs when $v = 0{\cdot}5$, and the two principal stresses are equally large.

2.2. MAXIMUM CROSS-SECTIONAL STRAIN ENERGY

The limits above for the maximum stress and strain in a point are expressed as functions of the strain energy density. In this section, the points on the cylinder cross-section where the strain energy is maximized are identified and limits for these maxima are found to be proportional to the cross-sectional average of the strain energy density.

The strain and stress given in equations (4) and (6) are linearly varying functions of z and consequently the maxima for strain and stress occur either on the inside or outside of the pipe wall, i.e., when $z = \pm T_c/2$.

The value of ϕ for which the strain energy density is maximized is found when it is recognized, see equations (4) and (13), that this function can be expressed as

$$e_p(x, \phi, \pm Tc/2) = C_1(x)\cos^2(n\phi) + C_2(x)\sin^2(n\phi). \tag{19}$$

Dependent on the values of the (unknown) positive functions C_1 and C_2, the maxima of this function are either where $\cos(n\phi) = 1$ or where $\sin(n\phi) = 1$. These maxima are given by

$$\max_\phi(e_p(x, \phi, \pm Tc/2)) = \max(C_1, C_2), \tag{20}$$

from which it is concluded that, for each trigonometric order n,

$$e_p(x, \phi, \pm Tc/2) \leqslant 1/\Lambda_n \langle e_p(x, \phi, \pm Tc/2)\rangle_\phi, \tag{21}$$

where $\langle\ \rangle_\phi$ denotes averaging over ϕ and where

$$\Lambda_0 = 1; \quad \Lambda_n = 1/2, \quad n \geqslant 1. \tag{22}$$

If there are several trigonometric orders present and they are assumed uncorrelated, the estimated value of the maximum e_p is still given by equation (21). However, the maximum possible value of e_p is

$$\max_\phi(e_p(x, \phi, \pm Tc/2)) \leqslant N/\Lambda_n \langle e_p(x, \phi, \pm Tc/2)\rangle_\phi, \tag{23}$$

where N is the number of trigonometric orders that are excited. This maximum value results if the strain energy densities of all the trigonometric orders are equal and if they all are maximized at the same value of ϕ, at the same time. This requires fully coherent sources, for example a point source. However, as the different trigonometric orders travel with different velocities, their relative phases will vary with frequency, unless the source is very peculiar. Therefore, for broadband excitation several wavelengths away it is reasonable to assume that the different trigonometric orders are incoherent, allowing equation (21) to be applicable on average.

It should be remembered, though, that if the trigonometric orders are coupled by the boundary conditions, for instance if the pipe is supported only at one point, equation (23) might apply. In this study, only homogeneous boundary conditions of the first and second kind are considered and these do not couple the trigonometric orders, so equation (21) is tentatively assumed to be valid also for coherent excitation.

The limits of maximum strain and stress are expressed above as functions of the strain energy density at $z = \pm T_c/2$ averaged over the circumferential. The next step is to express these limits as functions of the averaged cross-sectional strain energy

density. To that end, consider

$$\frac{1}{\Lambda_n E'}\langle e_p(x,\phi,\pm Tc/2)\rangle_\phi = \left(\left|\varepsilon_x \pm \frac{T_c}{2}\kappa_1\right|^2 + \left|\varepsilon_\phi \pm \frac{T_c}{2}\kappa_2\right|^2 + 2\nu\mathrm{Re}\left(\left(\varepsilon_\phi \pm \frac{T_c}{2}\kappa_2\right)^*\left(\varepsilon_x \pm \frac{T_c}{2}\kappa_1\right)\right) + g\left|\gamma \pm \frac{T_c}{2}\tau\right|^2\right)$$

$$\leqslant 4\left[(|\varepsilon_x|^2 + |\varepsilon_\phi|^2 + 2\nu\mathrm{Re}(\varepsilon_\phi^*\varepsilon_x) + g|\gamma|^2) + \frac{T_c^2}{12}(|\kappa_1|^2 + |\kappa_2|^2 + 2\nu\mathrm{Re}(\kappa_1^*\kappa_2) + g|\tau|^2)\right]$$

$$= \frac{4}{\Lambda_n E'}\langle e_p(x,\phi,z)\rangle_{\phi,z}, \tag{24}$$

where the average over z is calculated, as in the derivation of the Arnold and Warburton cylinder theory [17], by neglecting the trapezoidal form of the cylinder cross-section. The factor of four in the inequality results as, for any a and b, $|a + \sqrt{3}b|^2 \leqslant 4(|a|^2 + |b|^2)$. In equation (24), the left- and right-hand sides are equal if the in-plane strain is a factor $1/\sqrt{3}$ less than the flexural strain, in each of the four terms. For propagating radial-axial waves, below the ring frequency this is not the case. For these waves, the dominating terms in the strain energy density are the in-plane axial, circumferential flexural and flexural shear [19]. These terms appear in different terms on the left-hand side of equation (24). Thus, using the right-hand side of the equation for estimating stress, in many cases, leads to an overestimation of a factor in the range of $2/\sqrt{3}$ to 2, as compared to the left-hand side. However, the result leads to the beneficial conclusion that the maximum stress in a cross-section of a cylinder is limited by an expression that is proportional to the square root of the cross-sectional average of the strain energy density.

2.3. DISTRIBUTION OF STRAIN AND STRESS ALONG THE CYLINDER

Hamilton's principle states that the true motion of a system is the one that minimizes the time-averaged difference between potential and kinetic energy. For two important cases this difference is zero. Thus, for a wave in an infinite cylinder the time averages of the kinetic and the potential cross-sectional energy densities, for any x, are equal. Also, for a finite cylinder performing free vibrations and obeying any of the classical boundary conditions (i.e., homogeneous boundary conditions of the first or second kind), the time average total kinetic and potential energies are equal.

The classical boundary conditions are characterized by zero work, thus no exchange of energy, at the boundary. For the practically useful case of a "long" pipe (many wavelengths) the same condition may apply within the pipe. At frequencies

below half the ring frequency and above cut-on for each $n \geqslant 1$, there are only two real solutions to the dispersion relations for cylinders corresponding to a right and a left going wave respectively. In addition, there are six solutions corresponding to "nearfield" terms. These nearfield terms are found in the vicinity of the excitation and boundaries, decaying exponentially away from irregularities. This means, within the pipe at a point x between a boundary and the excitation, there are only two waves present. If the boundary condition is conservative and the damping is not large, the amplitudes of these two waves are equal. Consequently, the vibration field in such a point is

$$u = u_n \sin(\lambda_n x + \alpha_n)\cos(n\phi), \qquad v = v_n \cos(\lambda_n x + \alpha_n)\sin(n\phi),$$
$$w = w_n \cos(\lambda_n x + \alpha_n)\cos(n\phi), \tag{25}$$

where λ_n is found from the dispersion relations as are the relative amplitudes u_n/w_n and v_n/w_n. The phase constant α_n is governed by the nearest boundary condition, at $x = 0$. The amplitude w_n is determined by the excitation and by the boundary conditions at the other end.

Langley derived expressions for the energy flow in cylindrical shells [20, equations (21)–(29)]. By merely inspecting these expressions, considering a displacement field of the form (25), it is seen that the reactive work in the pipe is zero at the nodes of the radial displacement which are given by

$$\cos(\lambda_n x + \alpha_n) = 0. \tag{26}$$

(If losses are present there will, however, be a small active energy flow to balance the energy dissipation in the pipe between the considered point and the boundary.)

This quite lengthy discussion leads to two interesting conclusions. First, consider a pipe section in-between the boundary and a nodal point, as given by equation (25), located at least one or two wavelengths away from the boundary. Such a pipe section is from a reactive point of view energetically isolated from the rest of the pipe. Thus, Hamilton's principle applies for this section and the average potential and kinetic energies are equal. Second, for the vibration field in such a section, the excitation and the boundary conditions at the other end are only reflected by the amplitude of the (comparatively few) incoming waves. Because of this, the concentration of stress at a boundary may be investigated without considering the excitation and the other boundary condition in detail.

2.4. RELATING MAXIMUM STRESS TO AVERAGE VIBRATION VELOCITY

In the previous sections, first the maximum strain and stress were found to be limited by expressions proportional to the square root of strain energy density. Then the strain energy density was found to be limited by an expression proportional to its cross-sectional average. It was shown that the average strain energy within a pipe section, extending one or a few wavelengths from a boundary, is equal to the average kinetic energy within this section.

The kinetic energy density in a thin-walled pipe is

$$e_k = \tfrac{1}{2}\rho\omega^2(|u|^2 + |v|^2 + |w|^2). \tag{27}$$

Considering the radial-axial modes ($n \geqslant 1$), for frequencies well below the ring frequency, the axial in-plane inertia may be neglected and the cylinder motion is almost inextensional. Then the cross-sectional average kinetic energy density, to a good approximation, is proportional to the square of the radial velocity [19]

$$\langle e_k \rangle_{\phi,z} = \tfrac{1}{2} A_n \rho\omega^2 |w|^2(1 + 1/n^2). \tag{28}$$

It is then hypothesized that the maximum strain at a boundary is given by

$$(|\gamma|_{\max})^2 \leqslant 2(e_p)_{\max}/E = konst^* \rho/E\langle\omega^2|w|^2\rangle, \tag{29}$$

where $\langle\ \rangle$ denotes spatial average and where the non-dimensional constant *konst* is dependent on frequency and boundary condition. It may also depend on excitation and the relative amplitudes of the incoming waves of different trigonometric orders in which case the hypothesis is not effective. However, for boundary conditions that are separable in x and ϕ and for pipes where the excitation is several wavelengths away from the boundary, the arguments above support the idea of an effective and descriptive non-dimensional number.

Upon this basis, a non-dimensional strain factor Γ is defined,

$$\Gamma = |\gamma|_{\max}\frac{c_L}{V}, \quad c_L = \sqrt{E/\rho}, \quad V = \sqrt{\langle\omega^2 w^2\rangle}. \tag{30}$$

Following Hunt [7] it is seen that for a rod $\Gamma = \sqrt{2}$. Within a rectangular beam $\Gamma = \sqrt{6}$ whereas at a blocked end of a beam, according to Hunt, it is an additional 40–65% higher. Karzub and Norton published a list for the relation between maximum velocity and maximum strain [14]. When the trigonometric orders are uncorrelated, the maximum vibration velocity within a pipe (neglecting nearfield effects) is twice the root mean square (r.m.s.) average velocity. Upon this basis, the value given in reference [14] for cylinders corresponds to $\Gamma = 4$, whereas the value calculated in section 3 is $\Gamma \approx 6$.

3. EXPERIMENTS

Experiments are made on a pipe to verify that the maximum strain in a pipe is proportional to the r.m.s. average vibration velocity and to find the constants of proportionality. It was expected that the classical boundary condition responsible for the largest strain concentration is that where all displacement components are blocked. To facilitate the application of this boundary condition a lightweight plastic (drain) pipe was chosen for the experiments.

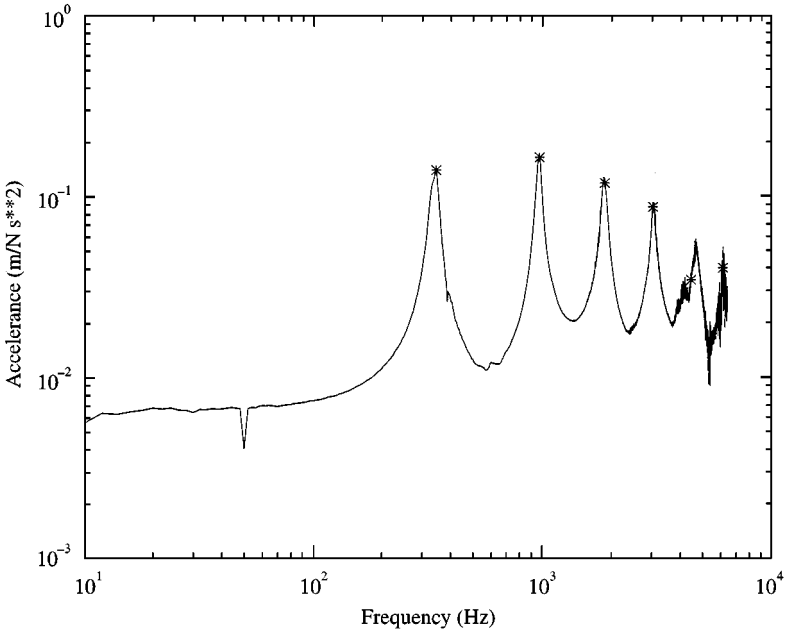

Figure 2. Accelerance of ring cut from plastic pipe. *, cut-on frequencies, equation (31), with Young's modulus obtained from a curve fit.

In what follows, the relation between the average vibration velocity of the pipe and the strain at the blocked end is estimated from measurements. The results are compared with those from calculations with the spectral finite element method presented in reference [4]. Preliminary measurements are made to determine the material data of the plastic pipe. Also, to verify the spectral FE-code, the results of a simple response calculation are compared to measurements.

3.1. PIPE DATA

A 2 cm section of the pipe was suspended on a thin elastic string and the accelerance was measured using a lightweight accelerometer and an impact hammer. Figure 2 shows the transfer accelerance to a point 180° from the force.

The resonance frequencies of a thin-walled ring given by [21]

$$f_n^2 = \beta \frac{n^2(n^2-1)^2}{1+n^2} \frac{E/\rho}{(2\pi R)^2}, \quad \beta = \frac{T_c^2}{12R^2}, \tag{31}$$

are used to estimate the Young's modulus with a least-squares fit to the first three resonances, corresponding to $n = 2$, 3 and 4. The experiment also verifies the use of linear thin-walled theory for describing the plastic pipe.

The pipe loss factor is estimated from the rings point mobility using the 3 dB bandwidth for the first four resonances.

TABLE 1
Pipe data

E (N/m^2)	ρ (kg/m^3)	v	R (mm)	T_c (mm)	η_e	η_v
$3{\cdot}55 \times 10^9$	$1{\cdot}43 \times 10^3$	0·4	33	1·9	0·025	0·01

The response calculation, described in section 3.2 below, was initially made with Poisson's ratio, $v = 0{\cdot}3$. This resulted in slightly too low cut-on frequencies for the higher order radial-axial modes, when compared to measurements. The resonance frequencies for the $n = 1$, beam modes, are almost independent of the Poisson ratio while for the $n \geqslant 2$ modes, the cut-on frequencies are proportional to $1/\sqrt{1 - v^2}$ [19]. Using this, an improved estimate of the Poisson ratio is obtained as $v = 0{\cdot}4$.

The data for the pipe are given in Table 1 and are used in the calculations.

3.2. PIPE VIBRATION RESPONSE

The plastic pipe was suspended by two elastic strings. Vibrations were excited by an impact hammer and the acceleration was measured with a lightweight accelerometer. The signals were high-pass filtered to reduce the low-frequency pendulum contribution to the measurements. The experiment was also simulated with the spectral FE program [4] using a frequency resolution of 1 Hz, as with the measurements. The calculations neglected the fluid loading from the air.

Figures 3–5 show the measured and calculated point mobility, input power from the point source and transfer mobility. At very low frequencies, the frequency resolution is too coarse to accurately display the peak value at resonance. At high frequencies, it appears as if the damping and stiffness of the laboratory pipe increases, as for the ring in Figure 2. Despite these frequency variations, the agreement between measured and calculated vibration response justifies the spectral FE code.

3.3. STRAIN CONCENTRATION AT A BLOCKED END

3.3.1. *Measurement procedure*

A 100 mm long solid steel cylinder was "push-fitted" into the plastic pipe and then glued to a heavy plate to block the pipe motion at the end. The other end of the pipe was suspended in an elastic string.

Vibrations in the pipe were excited with a small coil and magnet vibrator that was fed with pseudo-random noise. To get a reasonable signal-to-noise ratio also at higher frequencies the noise amplitude was increased with 2 dB/octave from 100 Hz.

The strain at the blocked end was measured with strain gauges developed by Liu and Pinnington [22, 23]. These gauges are made from piezo-electric film that is

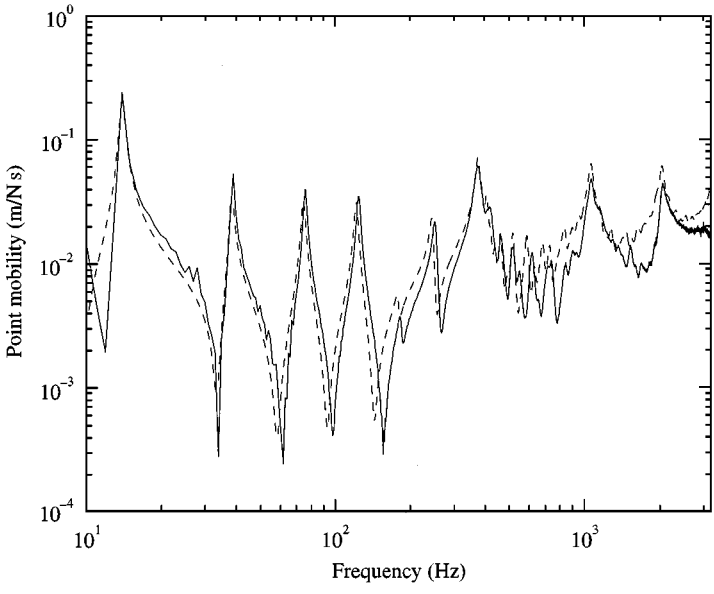

Figure 3. Magnitude of point mobility of plastic pipe; ——, measured; – – –, calculated.

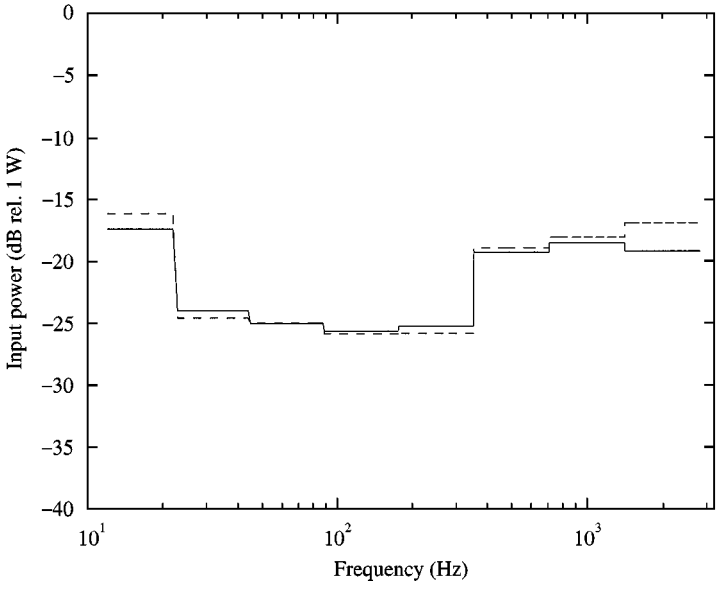

Figure 4. Octave band averaged Input Power to plastic pipe: ——, measured; – – –, calculated.

folded so that they are sensitive only to strain in one direction. They have higher sensitivity than usual wire gauges and linearity even at higher frequencies. Another advantage is that the signals are conditioned with the same type of charge amplifier that is used for accelerometer measurements; this is convenient and gives a good phase match between measurement channels.

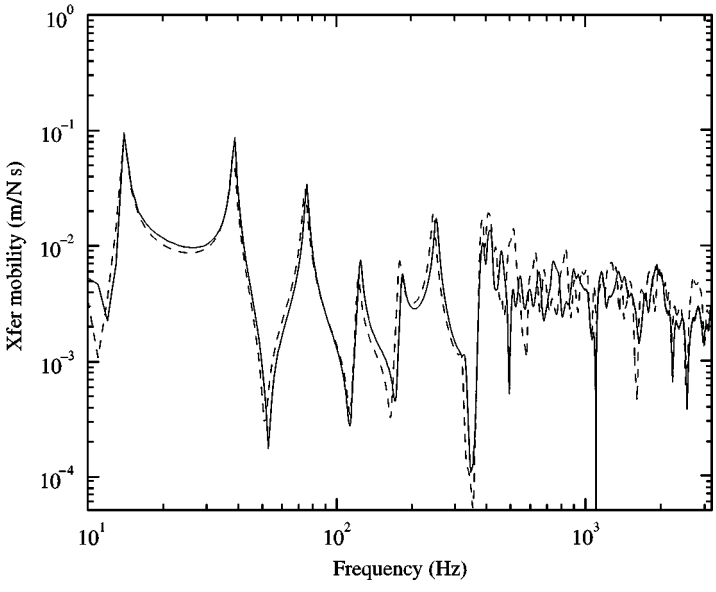

Figure 5. Magnitude of transfer mobility in plastic pipe: ——, measured, – – –, calculated.

The strain gauges were fitted to the pipe with double-sided tape and were screened with aluminium foil on the outside of the pipe. One of the major disadvantages with these gauges is that they are very sensitive to electromagnetic fields and despite the screening the measurements were quite noisy. (In the results shown below, the 50 Hz component is suppressed by setting it to the average of the measured value at 48 and 52 Hz). Liu calibrated carefully [22]. The calibration of the strain gauges [23] was confirmed by comparison with a standard strain gauge that was glued to the pipe.

Five strain gauges were randomly positioned at the blocked end—three in the axial direction and two in the circumferential direction. Accelerometer positions were chosen at random within a segment of the pipe starting one pipe diameter away from the blocked end and extending approximately 1 m towards the excitation. For each of the strain gauges, the transfer functions between strain and acceleration in four positions were measured. The accelerometers were then moved and the measurements repeated. The eight transfer functions were then integrated, their r.m.s. average was calculated and finally the result was inverted so that an estimate of the ratio of the strain to the average vibration velocity was found.

Figure 6 shows a typical accelerometer and strain measurement. Also shown is the coherence, which is quite low at frequencies where the strain is small. Figure 7(a) shows the strain factor, equation (30), for the three axial and Figure 7(b) for the two circumferential strain gauges. Figure 8 shows, for each of the three axial strain gauges, the relative standard deviation of the eight transfer functions between acceleration and strain. The relative standard deviation is of the order of 0·4 showing that, in this experiment, eight accelerometer readings are just about

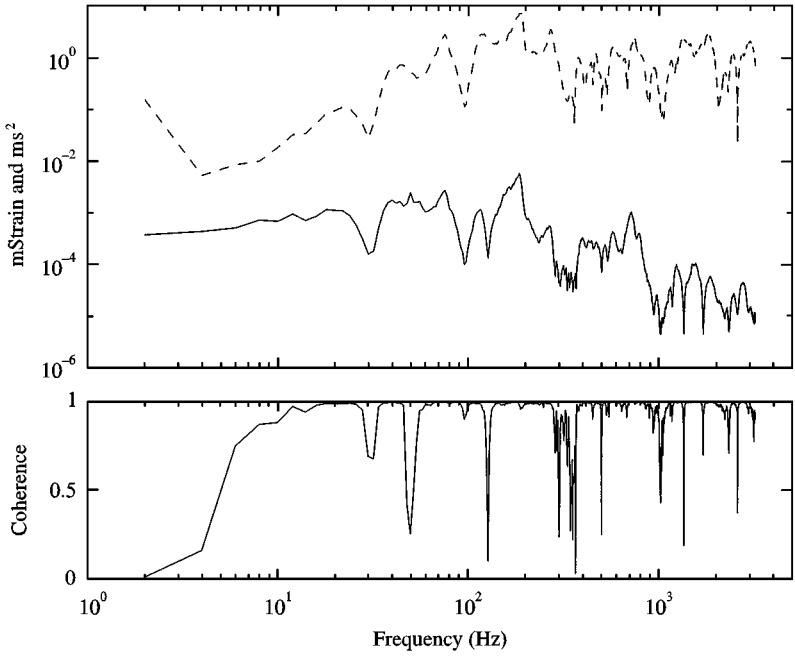

Figure 6. Upper, ——, strain at point 1 (in milli strain); – – –, acceleration of one accelerometer (m/s^2); lower, coherence.

enough for estimating the average vibration velocity. Thus, if the fact that eight readings are a small number is disregarded and the central limit theorem is applied, then the conclusion is that we are 90% confident that the average vibration velocity is correctly estimated within a factor of two.

The results in Figures 7 show that the strain varies with frequency, direction and position, giving in all cases the non-dimensional strain factor Γ of equation (30) less than five.

3.3.2. *Spectral finite element calculation*

The measurements are simulated with the spectral finite element method (SFEM) [4]. Using this method, the element formulation is remade for each frequency. The shape functions are a combination of the solutions to the equations of motion with a linear dependence on the displacements at the ends. For a pipe element, between $x = -L$ and L, the shape functions are

$$\begin{bmatrix} u \\ v \\ w \end{bmatrix} = \begin{bmatrix} \mathbf{B}_u \\ \mathbf{B}_v \\ \mathbf{B}_w \end{bmatrix} \operatorname{diag}(\exp(\alpha x - \alpha_p L)) \cdot \mathbf{A} \cdot [\mathbf{V}_1 \quad \mathbf{V}_2]^{\mathrm{T}}, \tag{32}$$

where the row vectors $\mathbf{B}_u$, $\mathbf{B}_v$ and $\mathbf{B}_w$ and the wave numbers α are found from the dispersion relations [4]. This means that any of the columns of the

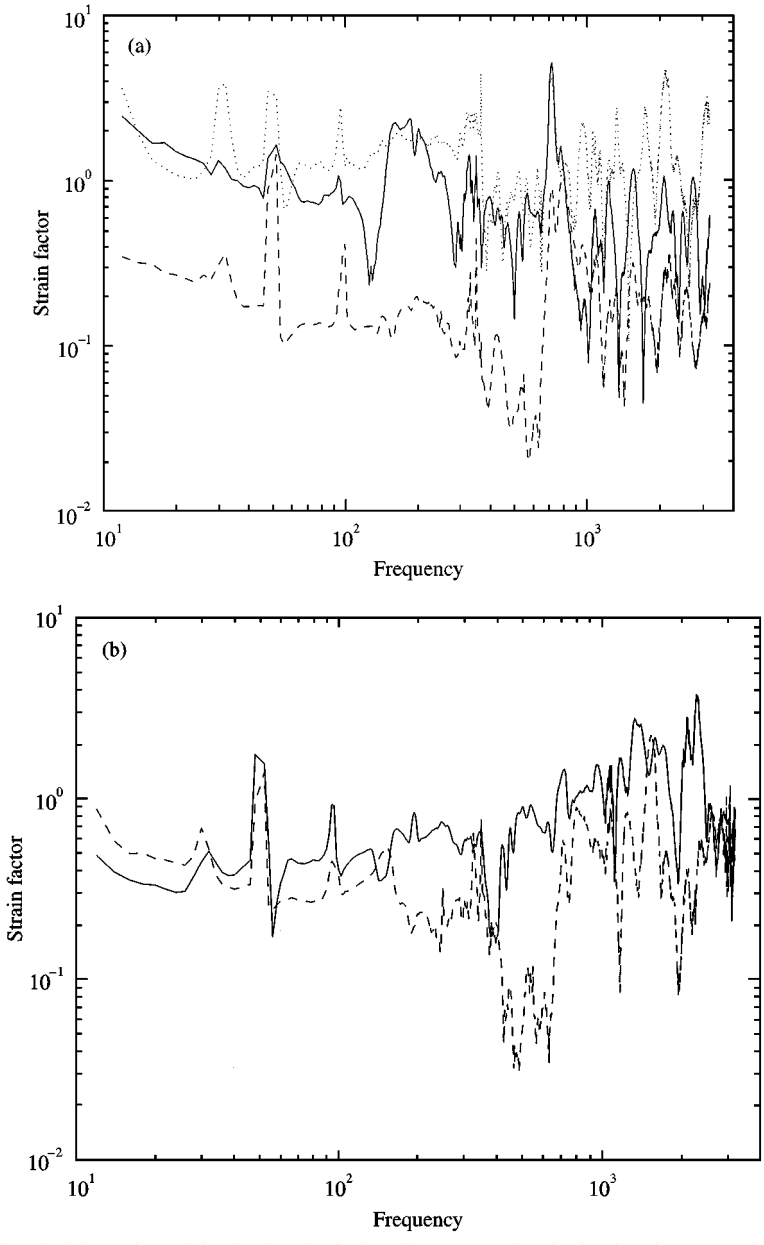

Figure 7. (a) Axial strain at blocked end of pipe times sound velocity in pipe material divided by r.m.s. radial vibration velocity. ——, Point 1; – – –, Point 2; ····, Point 3; (b) circumferential strain at blocked end of pipe times sound velocity in pipe material divided by r.m.s. radial vibration velocity; ——, Point 4; – – –, Point 5.

3×8 matrix

$$\begin{bmatrix} \mathbf{B}_u \\ \mathbf{B}_v \\ \mathbf{B}_w \end{bmatrix} \text{diag}(\exp(\alpha x)) \tag{33}$$

is an exact solution to the homogeneous equations of motion for the pipe.

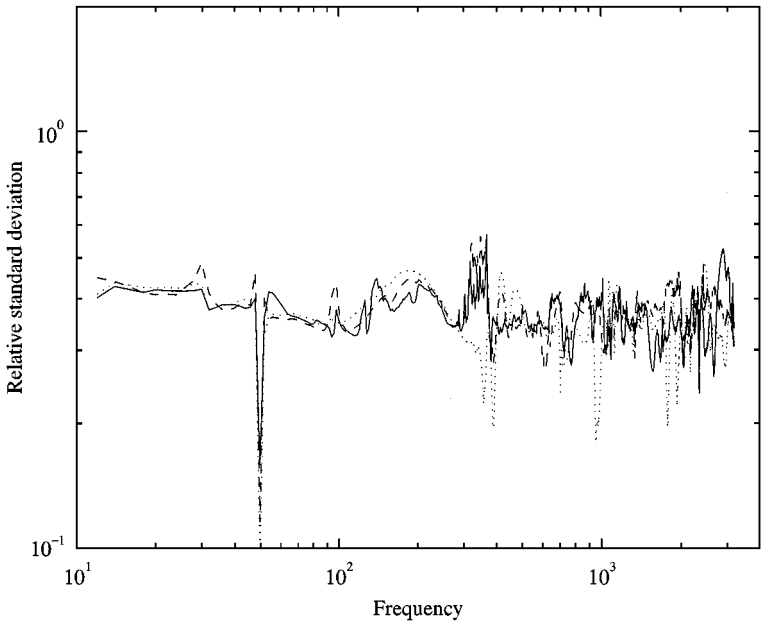

Figure 8. Relative standard deviation of estimated value of r.m.s. radial vibration velocity. Legends as in Figure 7(a).

In equation (32)

$$\alpha_p = \begin{cases} -\alpha & \text{if } \mathrm{Re}(\alpha) < 0, \\ \alpha & \text{otherwise,} \end{cases} \tag{34}$$

and

$$\begin{aligned} \mathbf{V}_1 &= [u(-L) \quad v(-L) \quad w(-L) \quad \partial w(-L)/\partial x], \\ \mathbf{V}_2 &= [u(L) \quad v(L) \quad w(L) \quad \partial w(L)/\partial x], \end{aligned} \tag{35}$$

whereas the matrix **A** is governed by the linear equation system resulting when the expression for the shape functions (32) is inserted into the boundary conditions (35).

The response of the pipe was calculated with the SFEM using the shape functions (32) in the element formulation. The excitation was a point force at a distance 2 m from the blocked end. Calculations were made for frequencies from 10 Hz up to 3·2 kHz with 2 Hz spacing (the same as in the measurements). The trigonometric orders $n = 0$ to 8 were considered. The major time consumption when using the SFEM is the calculation of the shape functions. Therefore, these are stored when the element formulation is made to ensure that the post-processing below is made efficiently.

3.3.3. *Average radial vibration velocity*

Once the nodal displacements $\mathbf{V}_1$ and $\mathbf{V}_2$ are known, the r.m.s. radial vibration velocity in a pipe segment, for the trigonometric order n, is given by

$$\langle(\omega w)^2\rangle = \frac{\Lambda_n \omega^2}{(X_2 - X_1)} \int_{X_1}^{X_2} |w|^2 \, \mathrm{d}x$$

$$= \frac{\Lambda_n \omega^2}{(X_2 - X_1)} [\mathbf{V}_1^* \; \mathbf{V}_2^*] \mathbf{A}^{\mathrm{H}} \cdot \mathrm{diag}(\mathbf{B}_w^*) \cdot \mathbf{E} \cdot \mathrm{diag}(\mathbf{B}_w) \cdot \mathbf{A} \cdot [\mathbf{V}_1 \; \mathbf{V}_2]^{\mathrm{T}} \tag{36}$$

where $*$ denotes complex conjugate, H denotes complex conjugate and transpose and where the matrix $\mathbf{E}$ is given by

$$\mathbf{E} = \mathbf{E}(\alpha, X_1, X_2, L) = \int_{X_1}^{X_2} \exp(\alpha x - \alpha_p L)^{\mathrm{H}} \exp(\alpha x - \alpha_p L) \, \mathrm{d}x. \tag{37}$$

The integral is calculated explicitly and upon this the $[i, j]$ element of the matrix $\mathbf{E}$ is

$$\mathbf{E}[i, j] = \frac{[\exp((\alpha^*[i] + \alpha[j])X_2) - \exp((\alpha^*[i] + \alpha[j])X_1)]}{\alpha^*[i] + \alpha[j]} \exp(-(\alpha_p^*[i] + \alpha_p[j])L). \tag{38}$$

3.3.4. *Maximum strain at the blocked end*

Using the standard FEM, because of increasing discretization errors when derivatives of the polynomial shape functions are calculated, the strains are not as accurately calculated as the displacements. However, with the shape functions (32) the derivatives needed for the strain are calculated explicitly without any errors. Consequently, from equations (4), (5) and (32), the strains are given by

$$\gamma_x(x, \phi, z) = \cos n\phi [\mathbf{B}_u \, \mathrm{diag}(\alpha) - z\mathbf{B}_w \, \mathrm{diag}(\alpha)^2] \cdot \mathbf{W},$$

$$\gamma_\phi(x, \phi, z) = \cos n\phi [(n\mathbf{B}_v + \mathbf{B}_w)/R + z(n\mathbf{B}_v + n^2\mathbf{B}_w)/R^2] \cdot \mathbf{W},$$

$$\gamma_{x\phi}(x, \phi, z) = \sin n\phi [-n\mathbf{B}_u/R + \mathbf{B}_v \, \mathrm{diag}(\alpha) - 2z/R(\mathbf{B}_v + n\mathbf{B}_w)\mathrm{diag}(\alpha)] \cdot \mathbf{W}, \tag{39}$$

where the vector $\mathbf{W}$ is

$$\mathbf{W}(x) = \mathrm{diag}(\exp(\alpha x - \alpha_p L)) \cdot \mathbf{A} \cdot [\mathbf{V}_1 \; \mathbf{V}_2]^{\mathrm{T}}. \tag{40}$$

The strains are calculated at the blocked end on the outside of the pipe, at $z = T_c/2$. The contributions for each trigonometric order $n = 0$ until $n = 8$ are calculated and summed. Then the largest eigenvalue of the strain tensor, equation (10), is calculated. This procedure is repeated for 180 equally spaced angular positions.

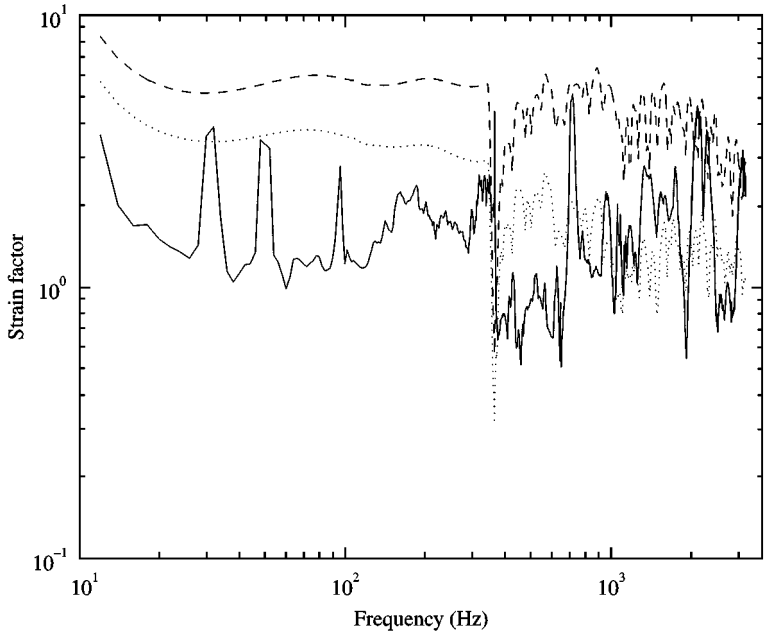

Figure 9. Maximum strain at blocked end of pipe times sound velocity in pipe material divided by r.m.s. radial vibration velocity. ——, estimated from five strain measurements; – – –, calculated; ····, calculated at a point 2 cm from the end.

Finally, the maximum strain at the blocked end of the pipe is found as the maximum of the largest principle strain in any of the 180 points along the circumferential.

3.3.5. *Results*

In section 2, equation (30), the non-dimensional dynamic strain factor Γ was defined as the maximum strain times the ratio of the sound velocity to the spatial r.m.s. radial velocity. The calculated dynamic strain factor is plotted in Figure 9. At low frequencies, Γ has an approximately constant value: $\Gamma \approx 6$. At very low frequencies, it increases somewhat as the part of the pipe where the motion is almost blocked, increases with the wavelength and therefore the calculated r.m.s. velocity in the section near the boundary becomes smaller. At higher frequencies, when the $n \geqslant 2$ modes are cut-on, the dynamic strain factor fluctuates. The different trigonometric orders are correlated as the incoming waves originate from the same point source. As the source is several wavelengths away and the trigonometric orders travel with different speed their relative phase varies rapidly with frequency and so does the maximum strain. The fluctuations, however, are not very large and the constant value $\Gamma \approx 6$ still applies on average. At frequencies above 1 kHz, there is a small drop in the strain factor, probably caused by damping. At high frequencies the energy density decays away from the source so that the vibration energy at the blocked end has decayed more than the average energy in the section where the velocity is calculated.

Also plotted in Figure 9 is the measured value of Γ. It is found by taking, for each frequency, the maximum of the five strain factors shown in Figure 7. The measured value fluctuates more than the measured and is consistently lower. There are three possible explanations for the differences: (1) The strain is measured only in one direction at five positions, hence it is very unlikely that the maximum strain in the cross-section is detected. Therefore, the measured value should be lower than the calculated. (2) It is difficult in practice to obtain a truly blocked boundary. Failure to achieve this will probably result in a lower strain factor. (3) The strain gauge length is approximately 2 cm, giving an average value rather than the strain exactly at the blocked end. For the frequencies considered there are, for each $n \geqslant 1$, eight solutions to the dispersion relations: two travelling waves (one in each direction), two exponentially decaying nearfield components and four "standing decaying waves". These last four correspond to wave solutions that are cut-on above the ring frequency, below which they have an approximately constant value. The slowest decay corresponding to the $n = 1$ wave is described by $\alpha \approx \pm 164 \pm \mathrm{i}158$ (1/m). This suggests a sharp decay from the blocked boundary leading to an underestimate of measured strain from a finite length gauge.

To investigate this last explanation for the difference between measured and calculated results, the strain factor was calculated 2 cm away from the blocked end. Figure 9 shows the measured and the two calculated strain factors, demonstrating that the exact positioning of the strain gauges influences the results. For the investigated pipe, the strain factor decreases approximately a factor $\sqrt{2}$ when a point slightly away from the boundary is considered.

As mentioned in the Introduction, Karzub and Norton have measured the ratio of maximum strain to maximum velocity [14]. They found a constant $K = 2$, which, since the maximum velocity for a pipe is twice the spatial r.m.s. value, corresponds to a strain actor $\Gamma = 4$. This is a factor $\sqrt{2}$ lower than the one found theoretically here indicating that a finite size strain gauge was used.

From the experiments, it is concluded that the maximum strain in a pipe can be estimated from accelerometer measurements. In addition, the great variability of the strain at the blocked end shows that it is difficult to find the maximum strain at a cross-section using strain gauges. In consequence, despite the uncertainty of the exact value of the factor Γ for "real-life" structures, the velocity method is not only more convenient, it can perhaps also be a more reliable method for finding maximum strain to predict fatigue life.

4. NUMERICAL EXPERIMENTS

Dimensional analysis shows the free vibration of cylinders to be a function of only four non-dimensional numbers

$$\beta = \frac{T_c^2}{12R^2}, \quad \Omega = \frac{\omega R}{c_L}, \quad n \text{ and } \nu, \tag{41}$$

where Ω is the non-dimensional frequency. Forced vibrations of finite cylinders, in addition to the four non-dimensional numbers in equation (41), also depend on the

excitation and on the boundary conditions. However, from the analysis in section 2.3, it follows that for a pipe that is several wavelengths long, the strain concentration at one end does not depend on the boundary condition at the other end. Similarly, the precise description of the excitation is not needed as it is only reflected by the amplitudes and phases of the incoming waves, one for each trigonometric order, which are uncorrelated for broadband excitation. Thus, if the trigonometric orders are not coupled by the boundary conditions, on average, they act independently at the boundary and the strain concentration does not largely depend on the excitation.

The numerical experiments are made with these considerations on a long pipe point excited at its middle. The total response for the trigonometric orders $n = 1$ to 25 is calculated. The experiment depends only on the non-dimensional numbers β, Ω and ν and on the boundary conditions at one end. By a systematic variation of these, the experiments presented below are a fairly complete study of the strain concentration in pipe structures.

4.1. INFINITE PIPE

An almost infinite pipe is investigated to give an idea of the strains within pipes. The pipe is 10^8 m long, the loss factors are $\eta_e = \eta_v = 10^{-5}$ while all other data are as given in Table 1. The maximum strain in a cross-section 125 m away from the excitation and the r.m.s. average radial velocity in a 5 m long section are calculated.

The dynamic strain factor is shown in Figure 10. At low frequencies, when only the $n = 1$ beam mode is cut-on, Γ has a constant value $\Gamma \approx 2$. At the cut-on frequency of the $n = 2$ mode, Γ increases by a factor $\sqrt{3(1 + 1/2^2)/2}$, as is explained in what follows.

At frequencies well below the ring frequency, the average cross-sectional average kinetic energy density is to a good approximation given by equation (28)

$$e_k = \Lambda_n \rho(\omega w)^2(1 + 1/n^2)/2. \tag{28}$$

Close to a modes cut-on frequency, the pipe response is dominated by this mode. At the cut-on of the $n = 2$ mode, the ratio of the square root of the kinetic energy to the radial velocity decreases by a factor $\sqrt{(1 + 1/2^2)/2}$ giving a corresponding decrease in strain factor. On the other hand, the strain energy in the $n = 1$ mode is entirely given by in-plane strain, whereas at the cut-on of a higher order mode the strain energy is predominantly flexural [19]. With reference to equation (24), the strain factor increases at cut-on by a factor $\sqrt{3}$. The combined effect of these two phenomena is that at cut-on of the $n = 2$ mode, $\Gamma \approx 2\sqrt{3(1 + 1/2^2)/2}$.

At a frequency $\sqrt{2}$ times the cut-on frequency, the strain energy becomes predominantly in-plane [24] so the strain factor decreases away from cut-on by a factor $\sqrt{3}$ compared to its maximum value at cut-on. At somewhat higher frequencies, the vibrations are controlled by both the $n = 1$ and 2 modes, so the strain factor fluctuates and increases to an intermediate value for the two modes.

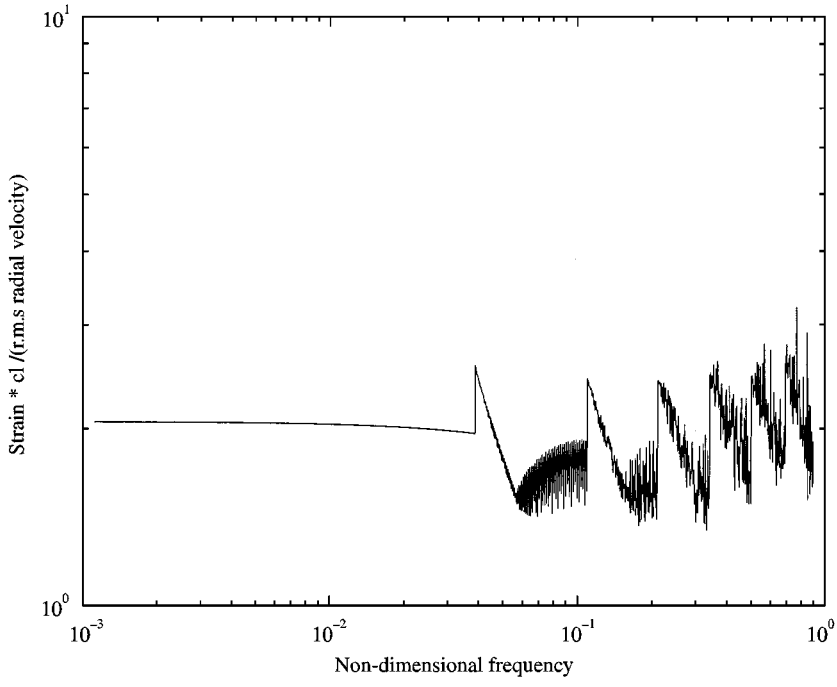

Figure 10. Strain factor in an infinite pipe.

This pattern repeats at the cut-on of the $n = 3$ and 4 modes, whereas at even higher frequencies the picture becomes less regular as the response is given by an increasing number of modes.

Despite the fluctuations discussed above, it is fair to draw the conclusion that within an infinite pipe the strain factor is limited in the range $1 < \Gamma < 4$. It is of the order $\Gamma \approx 2$ at low frequencies when only the $n = 1$ beam mode can propagate while, neglecting coherence effects, $\Gamma \leqslant 2\sqrt{3}$ at higher frequencies.

4.2. WITHIN A FINITE FLUID-FILLED PIPE

Within a reverberant finite pipe, for each cut-on trigonometric order there are two waves travelling in opposite directions. With two waves, instead of one wave, the r.m.s. velocity increases by a factor $\sqrt{2}$ while the maximum strain increases by a factor 2.

If in addition there is fluid within the pipe, for frequencies well below the cut-on of internal fluid modes, the cross-sectional average kinetic energy density is given by [19]

$$e_k = \Lambda_n \rho (\omega w)^2 (1 + 1/n^2 + 2\mu/n)/2, \quad \mu = R\rho_f / 2T_c \rho, \tag{42}$$

where ρ_f is the fluid density. This expression is a function of the trigonometric order n, while it is preferable to have it as a function of frequency. For frequencies where

the $n \geqslant 2$ higher order modes dominate the response, the $1/n^2$ (tangential in-plane inertia) term is small while the combined radial and fluid inertia terms are approximated as [24]

$$1 + 2\mu/n \approx (1 + 2\mu(2\mu\Omega^2/\beta)^{-1/5}). \tag{43}$$

Combining this with the results in the previous section, it is found that the strain factor within a finite fluid-filled pipe, for uncorrelated trigonometric orders, is approximately given by

$$\Gamma \approx \begin{cases} 2\sqrt{2}(1 + \mu), & f < f_{c2}, \\ 2\sqrt{6}(1 + 2\mu(2\mu\Omega^2/\beta)^{-1/5}), & f > f_{c2}, \end{cases} \tag{44}$$

where f_{c2} is the cut-on frequency for the $n = 2$ mode in [24]

$$f_{cn} = \frac{c_L}{2\pi R}\sqrt{\beta\frac{n^2(n^2-1)^2}{(1 + n^2 + 2n\mu)}}. \tag{45}$$

The strain factor estimate in equation (44) agrees with the measurements on oil-filled pipes presented by Norton and Fahy [11]. The rest of this paper considers only pipes without fluid.

4.3. STRAIN FACTOR AT THE END OF PIPES

For pipes described with thin-walled cylinder theory, four boundary conditions are required at each end. In this paper, homogeneous boundary conditions of the first and/or second kind are considered, that is, either the displacements or the force resultants are set to zero at the end. Thus, the four boundary conditions are [16]

$$\begin{aligned} u = 0 \quad &\text{or } N_x = 0, \\ v = 0 \quad &\text{or } S_{x\theta} = 0, \\ w = 0 \quad &\text{or } V_x = 0, \\ w_x = \partial w/\partial x = 0 \quad &\text{or } M_x = 0, \end{aligned} \tag{46}$$

where the explicit expressions for the force resultants N_x, $S_{x\theta}$, V_x and M_x are given in reference [16, equation (2.144), Tables 1.4 and 1.5]. However, they are not needed here since the spectral FE calculations are based upon a variational principle. Boundary conditions of the second kind are then natural boundary conditions, meaning that if no requirements are made on one of the displacement components, they will result in zero force.

The boundary conditions use the convention of Leissa [16, section 2.4.6], i.e., the blocked boundary condition is labelled (u, v, w, w_x) and the shear-diaphragm boundary condition is labelled (N_x, v, w, M_x).

A 200 m long pipe point excited at its middle is considered. The maximum strain at one end and the spatial r.m.s. average radial velocity in a section starting 1 m from the end and extending 5 m towards the source are calculated. The loss factors are $\eta_e = \eta_v = 10^{-6}$ at the pipe section where the strain is calculated and $\eta_e = \eta_v = 10^{-3}$ in the other section. Unless explicitly stated the other data are as specified in Table 1.

4.3.1. *Wall thickness*

To investigate the importance of the parameter β on the strain factor, three different wall thicknesses are considered: $R/T_c = 15$, 40 and 120. Calculations are made for the blocked boundary condition (u, v, w, w_x).

The calculated strain factors are plotted in Figure 11(a) for narrow bands and in Figure 11(b) for one-third octave bands. As found in section 3.3, at low frequencies the strain factor is a constant $4\sqrt{2}$. At cut-on of higher order modes, it first drops and then starts to fluctuate (because of coherence between different waves) and may become slightly larger. On average, the strain factor $\Gamma = 4\sqrt{2}$ applies while in this experiment it is limited to $\Gamma < 7$.

The factor $4\sqrt{2}$ may be obtained from the heuristic argument that: the strain factor within a pipe is $2\sqrt{2}$, this value applies at antinodes where the translational motion of the cross-section is not restricted while the cross-sectional rotation and the pipe wall rotation are zero. It then seems plausible that the strain doubles if the former motions are restricted. This argument is supported by the results in Figure 11(b).

4.3.2. *The Poisson ratio*

The dependence of strain factors on the Poisson ratio is investigated. The calculations are made, as in the previous section by considering a blocked boundary, for pipes with wall thickness $T_c = R/40$ and with the Poisson ratio $\nu = 0$, 0·3 and 0·5. The results are for clarity shown in 1/3-octave bands in Figure 12. As can be seen, the strain factor drops approximately by 30% for $\nu = 0$ while it is quite similar for $\nu = 0{\cdot}3$ and 0·5. It may then be concluded that the strain factor does not largely depend on the Poisson ratio.

4.3.3. *Other standard boundary conditions*

For pipes, there are in total 16 homogeneous boundary conditions of the first and second kind. The blocked boundary condition (u, v, w, w_x) is discussed above. The other three standard boundary conditions are the free (N_x, $S_{x\theta}$, V_x, M_x), the sliding (u, $S_{x\theta}$, V_x, w_x) and the shear diaphragm (simply supported) (N_x, v, w_x, M_x) boundary conditions. The strain factors for the remaining 12 boundary conditions are presented in section 4.4. Most of them are not easily realized in practise so the engineering significance of this investigation is perhaps limited. However, the results raise some interesting questions.

Figure 13 shows the strain factors for three standard boundary conditions, for a pipe with $\nu = 0{\cdot}3$ and $T_c = R/40$. The shear-diaphragm boundary condition

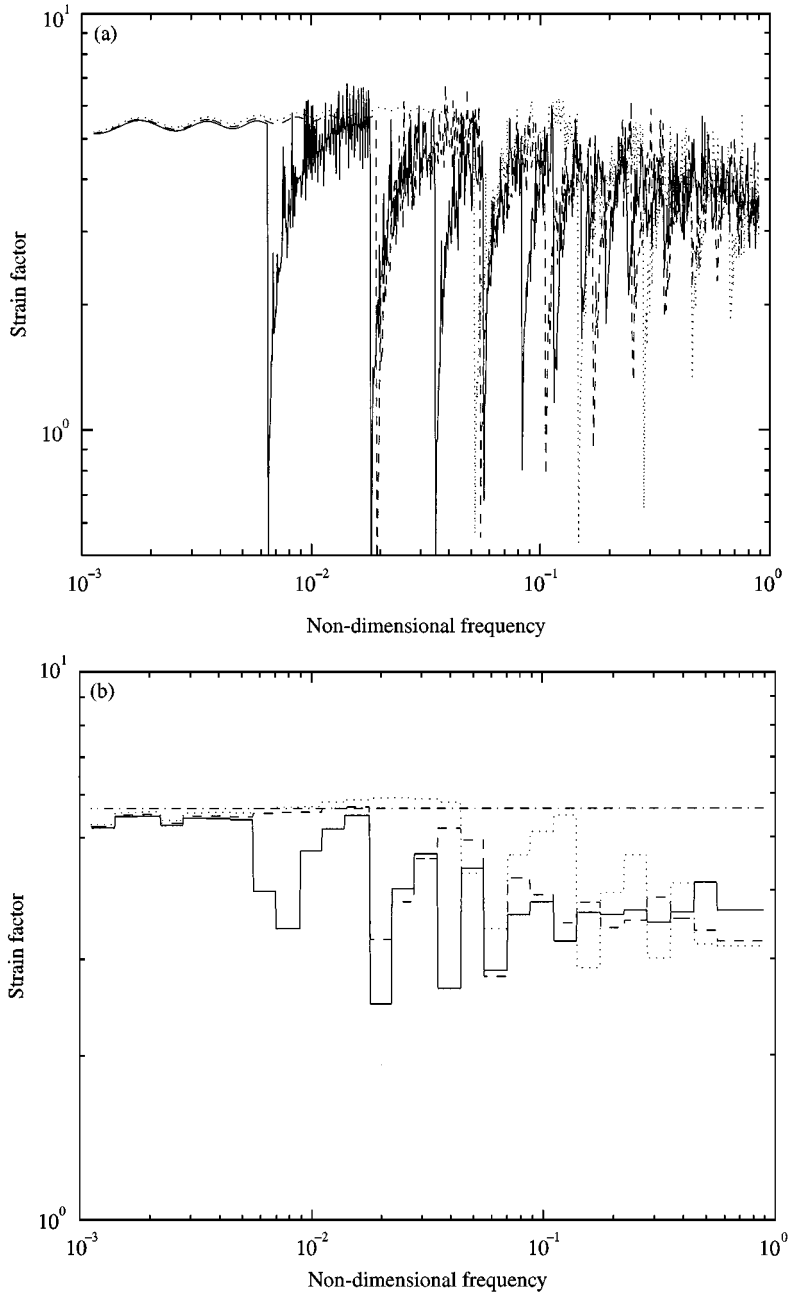

Figure 11. (a) Strain factor at blocked end. ——, $T_c = R/120$; – – –, $T_c = R/40$; ·····, $T_c = R/15$; (b) strain factor at blocked end in one-third octave bands: ——, $T_c = R/120$; – – –, $T_c = R/40$; ·····, $T_c = R/15$; – · – ·, $4\sqrt{2}$.

(N_x, v, w, M_x) is special in that it does not introduce any nearfield component [16]. At frequencies below the ring frequency, the $n = 1$ waves in pipes are described by the beam theory. For an Euler beam, the strain is zero at a simply supported end. Similarly, for a Timoshenko beam the axial in-plane strain is zero but, increasingly

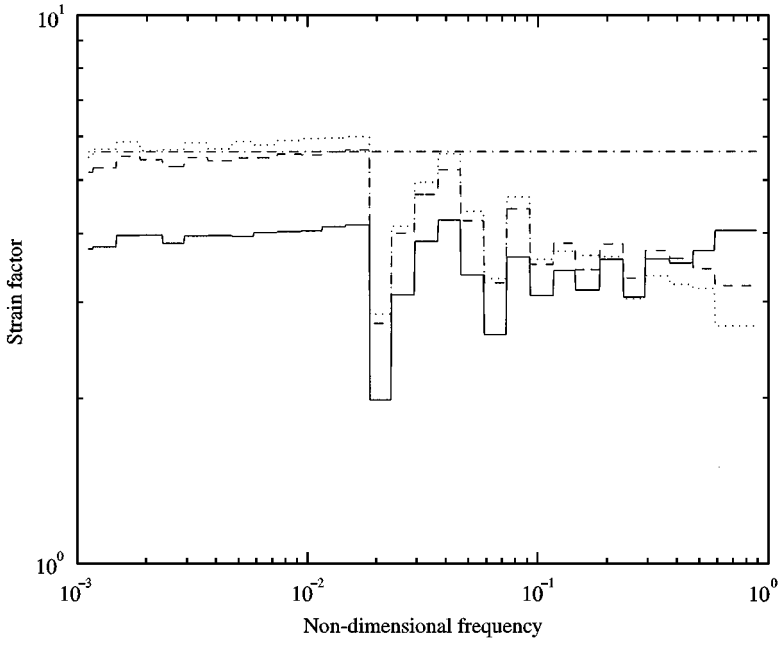

Figure 12. Strain factor at blocked end in one-third octave bands: ——, $v = 0$; – – –, $v = 0{\cdot}3$; ·····, $v = 0{\cdot}5$; – · – ·, $4\sqrt{2}$.

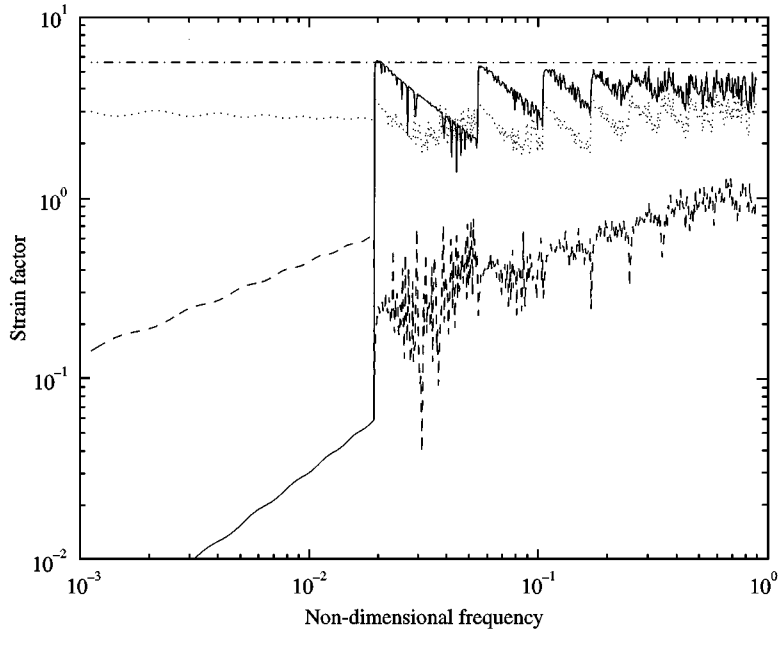

Figure 13. Strain factor: ——, at free end; – – –, at shear-diaphragm end; ····· , at sliding end; – · – ·, $4\sqrt{2}$.

with frequency, there is some in-plane shear strain. Apparently, see Figure 13, this also applies for pipes. At the cut-on of higher order modes the dominating terms in the strain energy are the circumferential flexural and in-plane axial strains. Both these terms are zero at a shear diaphragm end and therefore the strain factor drops at cut-on. But for frequencies close to the ring frequency, the strain factor at a shear-diaphragm end is smaller than the one that applies within pipes.

The strain factor for a free boundary (N_x, $S_{x\theta}$, V_x, M_x) is small at lower frequencies. At cut-on frequencies, where the circumferential flexural stain is large, the strain factor reaches the limiting value $\Gamma \approx 4\sqrt{2}$, the same that applies for a blocked boundary. Finally, the strain factor found for a sliding boundary (u, $S_{x\theta}$, V_x, w_x) has quite an undramatic behaviour and the same applies for all frequencies of the order of the one found within pipes.

In summary, the numerical experiments presented in this section show that, but for details in narrow bands, the strain factor is independent of wall thickness and has little dependence on the Poisson ratio. Additionally, if the maximum strain is sought at any point in the pipe, the strain factor is independent of both frequency and boundary condition, within a factor of two. Thus, for the four boundary conditions considered, the calculated strain factors are in narrow bands limited by $\Gamma < 7$ and on the average by $\Gamma \leqslant 4\sqrt{2}$. For some boundary conditions, the strain factor has its maximum within the pipe.

4.4. OTHER BOUNDARY CONDITIONS

The strain factors for four "standard" boundary conditions were calculated above. Figure 14 shows the strain factor for the remaining 12 homogeneous boundary conditions of the first or second kind.

In section 4.3.3, it was found that for the four boundary conditions considered the frequency-averaged strain factor is limited by $\Gamma \leqslant 4\sqrt{2}$. In section 2, it was argued that, since there is no reactive energy exchange at the end of a pipe where the boundary conditions are of the first or second kind, there should not be any local resonances and therefore the amplitude of the nearfield terms should not be substantially greater than the amplitude of the incoming wave and, consequently, the strain factor should be limited. It is seen from Figure 14 that this is not true for all homogeneous boundary conditions; the strain factor calculated from the strain at the boundary is not limited to $\Gamma \leqslant 4\sqrt{2}$. However, it is so limited for all boundary conditions when it is calculated from the strain 1 cm away from the boundary—$R/3 \approx 1$ cm.

For the boundary conditions (N_x, v, w, w_x), (N_x, v, V_x, w_x), (N_x, $S_{x\theta}$, w, w_x) and (N_x, $S_{x\theta}$, V_x, w_x), the strain factor increases at very low frequencies. All these boundary conditions have the rotation of the shell wall, w_x, restricted while the cross-sectional rotation, u/R, is free. Figure 15 shows for the boundary condition (N_x, v, w, w_x) the strains for the $n = 1$ mode in the pipe at $\Omega = 1{\cdot}26 \times 10^{-3}$ ($f = 10$ Hz) as functions of the distance from the boundary. Close to the boundary, the axial strain is large while it decreases exponentially at a rate corresponding to the real part of the standing decaying wave numbers ($\alpha = -248 \pm i245$ (1/m)).

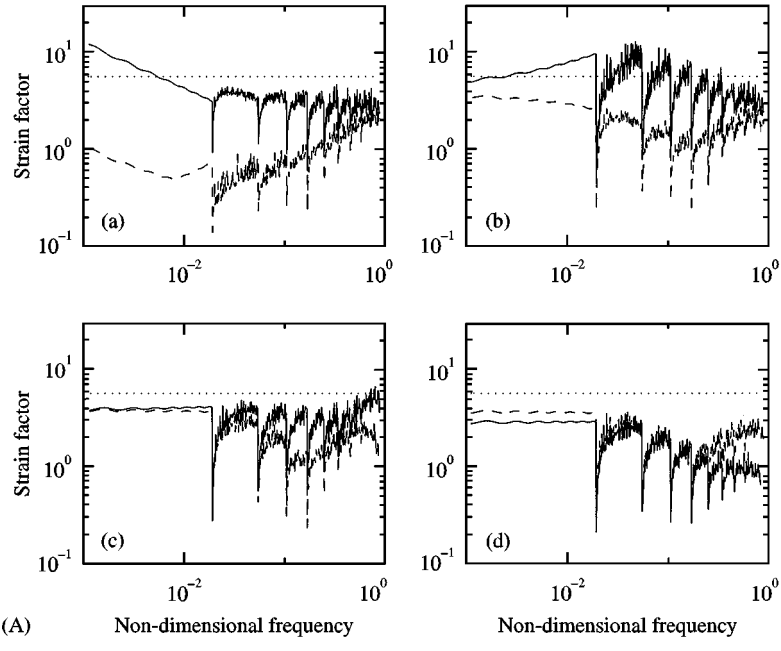

Figure 14. (A) Strain factor for different boundary conditions, $R/T_c = 40$, $\nu = 0{\cdot}3$, ——, at end; – – –, 1 cm from end; ····, $4\sqrt{2}$: (a) (N_x, v, w, w_x); (b) (u, $S_{x\theta}$, w, w_x); (c) (u v, V_x, w_x); (d) (u, v, w, M_x).

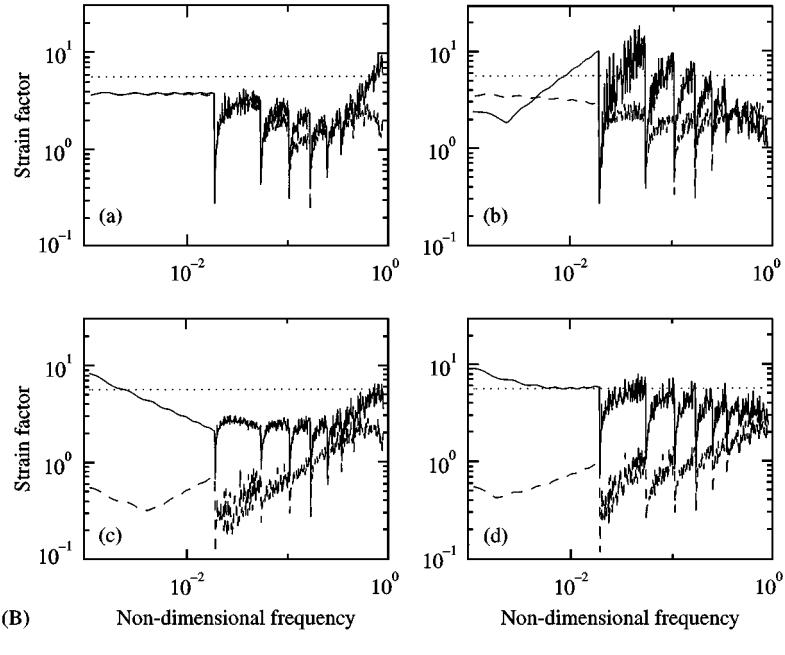

Figure 14. (B) Strain factor for different boundary conditions, $R/T_c = 40$, $\nu = 0{\cdot}3$, ——, at end; – – –, 1 cm from end; ····, $4\sqrt{2}$: (a) (u, v, V_x, M_x); (b) (u, $S_{x\theta}$, w, M_x); (c) (N_x, v, V_x, w_x); (d) (N_x, $S_{x\theta}$, w, w_x).

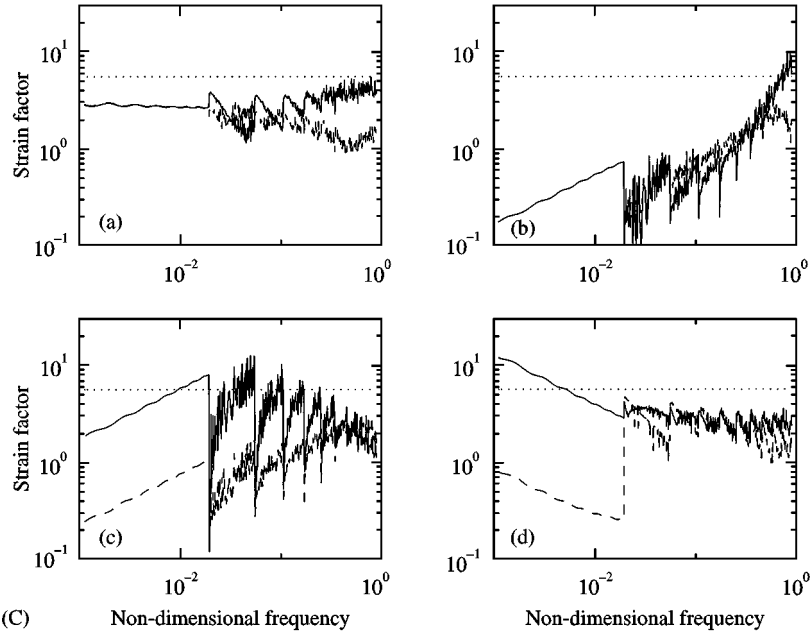

Figure 14. (C) Strain factor for different boundary conditions, $R/T_c = 40$, $\nu = 0{\cdot}3$, ——, at end; – – –, 1 cm from end; ····, $4\sqrt{2}$: (a) $(u, S_{x\theta}, V_x, M_x)$; (b) (N_x, v, V_x, M_x); (c) $(N_x, S_{x\theta}, w, M_x)$; (d) $(N_x, S_{x\theta}, V_x, w_x)$.

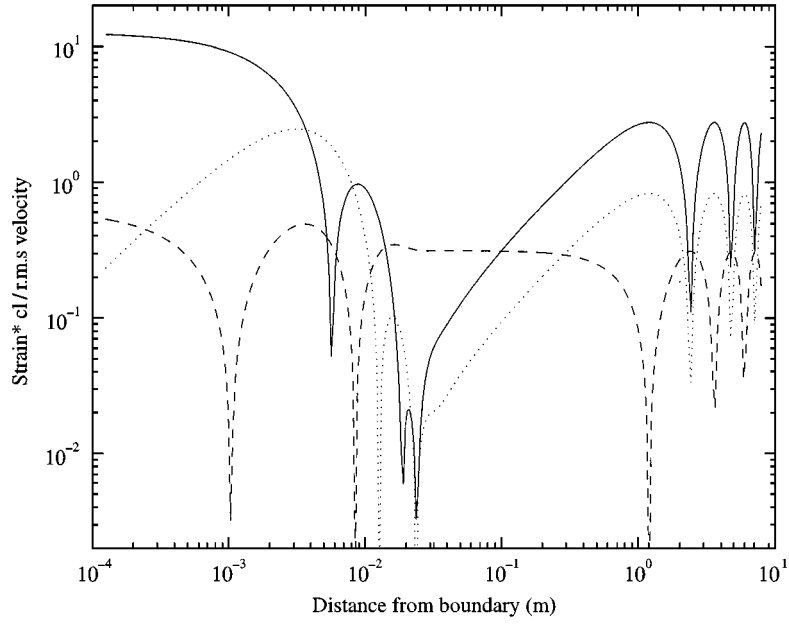

Figure 15. Amplitudes of strain on the outside of the wall in the $n = 1$ beam mode normalized with the ratio of the sound velocity to the r.m.s. radial vibration velocity, $R/T_c = 40$, $\nu = 0{\cdot}3$, boundary condition (N_x, v, w, w_x), $\Omega = 1{\cdot}26 \times 10^{-3}$: ——, axial strain; – – –, shear strain; ····, circumferential strain.

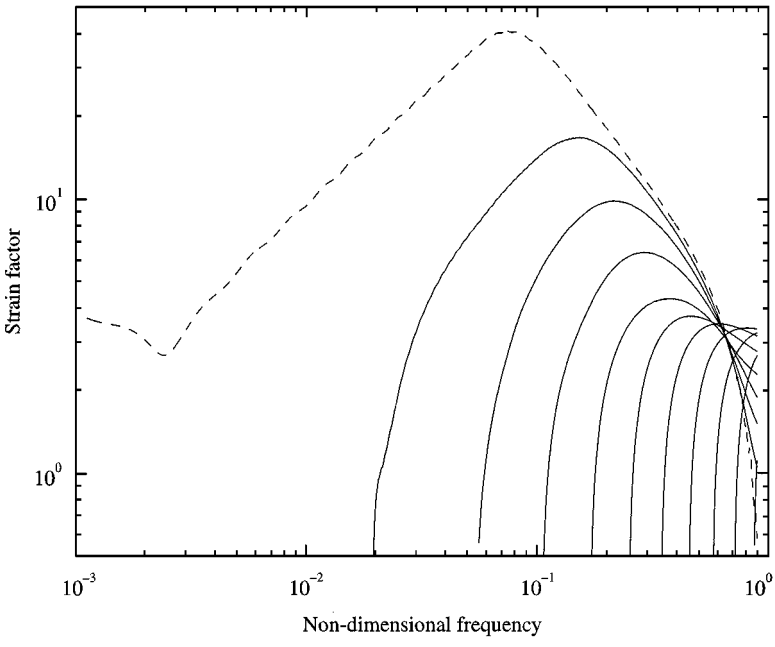

Figure 16. Strain factor for boundary condition $(u, S_{x\theta}, w, M_x)$, $R = T_c/40$, $\nu = 0{\cdot}3$; – – –, $n = 1$; ——, $n = 2, 3, \ldots, 12$.

For the boundary conditions $(u, S_{x\theta}, w, w_x)$, $(u, S_{x\theta}, w, M_x)$, $(N_x, S_{x\theta}, w, w_x)$ and $(N_x, S_{x\theta}, w, M_x)$, the strain factor increases at intermediate frequencies. These boundary conditions have the radial but not the tangential displacement blocked. In Figure 16, the strain factors are plotted for the trigonometric orders 1–12 for the boundary condition $(u, S_{x\theta}, w, M_x)$ showing that the large strain factor found in Figure 14(b) is predominantly due to the $n = 1$ mode.

Using beam theory for describing the $n = 1$ pipe vibrations, the motion restraints are that the tangential and radial displacements have equal magnitude and that, at low frequencies, the cross-sectional rotation is proportional to the slope of the radial displacement, i.e., to the shell wall rotation. The two groups of boundary conditions considered above do not fulfil both these restraints, so, the standing decaying waves are excited. This is verified by inspecting the relative amplitudes of the waves at the boundary showing that the standing decaying nearfield waves have a large amplitude when the strain factor is large. In Figure 15, it is noted that at a distance away from the boundary equal to the wall thickness (0·82 mm) the axial strain has decreased by 20%. This rapid decrease makes the application of thin-walled shell theory not entirely satisfactory. However, it is beyond the scope of the present work to doubt such theory.

In conclusion, for most boundary conditions, the strain factor is limited by $\Gamma \leqslant 4\sqrt{2}$. However, for some boundary conditions that are in conflict with the restraints on motion imposed by beam theory, the strain factor is larger than this. In these cases, there is a large concentration of strain decaying exponentially away from the boundary. The rate of decay is so rapid that it would be difficult to

measure it and as it seems difficult to find a practical situation where these boundary conditions are applied, the engineering significance of the finding of the large strain concentration is perhaps limited.

4.5. AXISYMMETRIC MODES

At frequencies below the ring frequency there are two $n = 0$ axisymmetric modes that can propagate, the in-plane longitudinal mode and the torsional mode. The $n = 0$ longitudinal mode is included in the analysis in Section 3 but, as its mobility is low for radial excitation, it does not much influence the results.

Both axisymmetric modes have different relations between radial velocity and kinetic energy from the one given in equation (28) which applies for the $n \geqslant 1$ radial–axial modes. The torsional mode has, using thin-walled cylinder theory, no radial motion. Thus, by definition, the strain factor defined in equation (30) is infinite for this mode. Similarly, there is some radial motion from "Poisson coupling" in the longitudinal mode; however, the strain factor would be very large if equation (30) was applied. So the velocity method cannot be used to detect strain associated with the axisymmetric modes if it is based on only radial accelerometer measurements.

An alternative would instead be to apply the velocity method with three-axial accelerometers estimating the total kinetic energy. The in-plane kinetic energy is low for the higher order radial–axial modes while it is approximately equal to the one for radial motion for the $n = 1$ mode. Thus, estimating the strain from the total kinetic energy should not much alter the results found in the previous sections.

Considering this, when large in-plane motion is expected the strain factor should be

$$\Gamma = (\gamma)_{\max} \frac{c_L}{V}, \quad c_L = \sqrt{E/\rho}, \quad V = \sqrt{\langle \omega^2 (u^2 + v^2 + w^2) \rangle}. \tag{47}$$

To investigate this idea, the strain factor in equation (47) is calculated for a pipe with $\nu = 0{\cdot}3$ and $T_c = R/40$. A blocked boundary is considered and the pipe is excited in turn with a radial, axial and transverse point force at its middle. Figure 17 shows the strain factors calculated when the $n = 0$ modes are considered. At low frequencies, the strain factors are large as the section where the kinetic energy is calculated is smaller than the wavelength so, because of the blocked boundary condition, the averaged kinetic energy in the pipe is underestimated. The strain factors for axial and radial excitations are identical, both these forces exciting the longitudinal but not the torsional mode. Apart from low frequencies, it has the almost constant value of $\Gamma \approx 2$, as for Hunt's analysis for rods [7]. The transverse force excites only the torsional mode and results in a strain factor $\Gamma \approx 2c_T/c_L = 2\sqrt{G/E}$.

Figure 18 shows the strain factor calculated for the three force excitations considering all the trigonometric orders 0–16. It is seen that the strain factors drop somewhat as compared to the results in Section 4.3. At low frequencies, when only

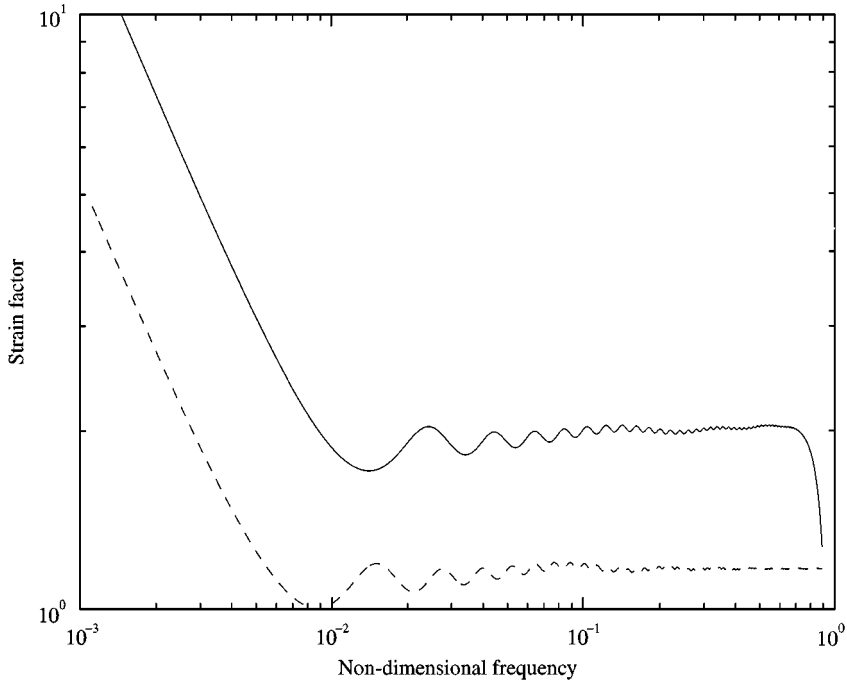

Figure 17. Strain factor at blocked end $R/T_c = 40$, $\nu = 0{\cdot}3$, $n = 0$: ——, axial and radial excitations; – – – –, tangential excitation.

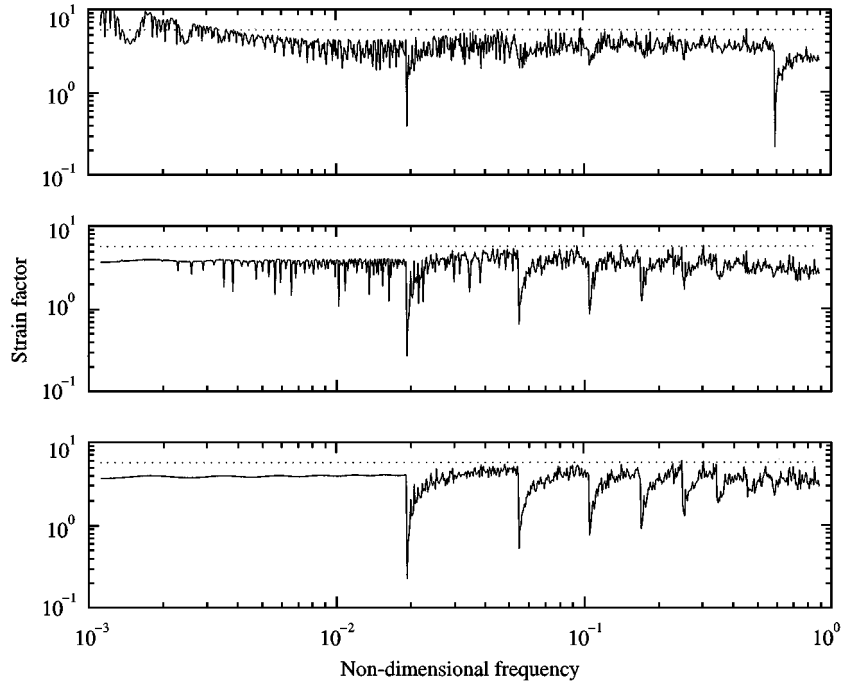

Figure 18. Strain factor at blocked end $R/T_c = 40$, $\nu = 0{\cdot}3$, $n = 0, 1, \ldots, 16$: ——, strain factor, equation (47); $\cdots$, $4\sqrt{2}$; top, axial excitation; middle, tangential excitation; bottom, radial excitation.

the $n = 1$ beam mode and the $n = 0$ axisymmetric modes can propagate, the strain factor based on equation (47) is approximately $\Gamma \approx 4$. At somewhat higher frequencies, when the $n \geqslant 2$ radial–axial modes can propagate, it increases to be approximately $\Gamma \approx 4\sqrt{2/(1 + 1/n^2)}$. Finally, for frequencies close to the ring frequency the restraints against in-plane motion decreases and the strain factor drops slightly.

In conclusion, when the axisymmetric $n = 0$ modes are excited, the velocity method for estimating dynamic strain must be based on the total kinetic energy as in equation (47). In this case, the strain factor will be dependent on those modes that dominate the response and thus it will be dependent on the excitation. It is $\Gamma \approx 1{\cdot}2$ for torsional modes, $\Gamma \approx 2$ for longitudinal modes, $\Gamma \approx 4$ for beam modes and finally it reaches $\Gamma \approx 6$ for higher order radial–axial modes. This range of values means that, without precise knowledge of the vibration field, it is difficult to predict fatigue life with the velocity method. However, it should still be very useful for assessing fatigue risk.

5. CONCLUSIONS

The velocity method for estimating strain in pipe structures is investigated. With this method, the predicted or measured spatial r.m.s. vibration velocity and theoretically derived strain factors are used to estimate maximum strain. Average vibration may be obtained for example from SEA. Alternatively, estimates of peak strain and hence fatigue life can be made from estimates of spatial average velocity obtained from a few monitoring positions.

Theoretical investigations are made showing that the strain in a point is limited by an expression proportional to the strain energy density which in turn is related to its cross-sectional average. For a reverberant field or for an infinite pipe, the average strain energy density is equal to the average kinetic energy density. For the radial–axial modes of order $n \geqslant 1$, the square root of the kinetic energy density is proportional to the radial vibration velocity. It is argued that the strain at a pipe end should be proportional to the amplitudes of the incoming vibrational waves and thus to the average energy density. Upon this basis, the non-dimensional "strain factor" Γ is defined as the maximum strain times the ratio of the sound velocity in the pipe material to the r.m.s. averaged radial vibration velocity. Measurements and numerical experiments are made to investigate whether the strain factor is an effective and descriptive non-dimensional number.

Measurements made at the blocked end of a plastic pipe show that the strain factor is an almost constant function of frequency with a value of the order of those previously reported [11, 14]. The strain measurements are made with piezo-electric film gauges that have high sensitivity and good linearity [22, 23]. The measurements are compared with calculations using the spectral finite element method presented in reference [4], here developed by routines for calculating average vibration response and for calculating strain and stress. The results agree very well, this justifying numerical simulation of the strain concentration in pipes.

Pipe vibration is a function of only four non-dimensional numbers, the excitation and the boundary conditions. For long pipes, the strain at one end depends only on

the boundary conditions at the other and on the excitation via the amplitudes of the relatively few incoming waves. If the excitation is of random and broadband character, the incoming waves are uncorrelated. Then the strain factor can be calculated without considering the excitation and the boundary conditions at the other end in detail. Considering this, numerical experiments are made on a long pipe excited by a point force at its middle. A deterministic point force is used as it provides a check on the sensitivity of the results on the assumption of uncorrelated excitations.

The four non-dimensional numbers, n, ν, β and Ω and the boundary conditions are all varied. It is found that for blocked boundary conditions the trigonometric order, the Poisson ratio, wall thickness and frequency only have a limited influence on the strain factor. All possible homogeneous boundary conditions of the first and second kind, 16 in all, are considered. For most of these boundary conditions, the strain factors are limited by the value for the blocked boundary condition: $\Gamma \approx 6$. For some of the boundary conditions, the largest strain is found within the pipe; the strain factor is then reduced by approximately a factor of two.

The $n = 0$ axisymmetric modes have no or little radial motion so, when these modes are excited, the velocity method has to be based on the total kinetic energy density including the in-plane motion. This can be accomplished with three-axial accelerometer measurements. Numerical experiments are made showing that the velocity method, based on total r.m.s. vibration amplitude, can be used to simultaneously detect the maximum strain for both in-plane and out-of-plane modes. However, the calculated strain factors depend on which modes that are excited, ranging from $\Gamma \approx 1{\cdot}2$, for the torsional mode, to $\Gamma \approx 6$, for higher order radial–axial modes. This range of values means that it is difficult to predict fatigue life with the velocity method. However, it should still be very useful for assessing fatigue risk.

For two groups of boundary conditions, the strain factors exceed the one for the blocked boundary. The large strain factors are found for the $n = 1$ beam mode when the boundary conditions are in conflict with the restraints on motion imposed by beam theory. These restraints are: the amplitudes of tangential and radial displacements are equal and, at low frequencies when Euler beam theory is valid, that the cross-sectional rotation (axial displacement divided by the radius) is equal to the shell wall rotation (the slope of the radial displacement). Beam theory describes the waves within pipes with high accuracy when compared to shell theory [19]. Thus, if the restraints on motion put up by beam theory are in conflict with the additional boundary conditions required by shell theory, the additional waves that are found for shells are excited. These solutions are "standing decaying waves" with high wavenumbers, i.e., rapidly decaying oscillating functions. This reasoning is confirmed with numerical experiments where high strain concentrations, caused by standing decaying waves, are found when the boundary conditions are that the tangential displacement is free while the radial displacement is blocked. High strain concentrations are also found for low frequencies if the axial displacement is free and the rotation of the shell wall is blocked.

The boundary conditions discussed above are rarely found in pipe works. Thus, the existence of large strain factors does not greatly restrict the practicality of the

velocity method for finding maximum strain at the end of pipes. However, pipes often fail at small bore connections and at unsupported masses, e.g., at T-junctions, flanges pressure gauges and valves. Such connections may well introduce conditions on motion that are similar to those that applies for the boundary conditions discussed, this possibly resulting in high strain concentrations. Indeed, for flanges at the frequency of total transmission, large vibrations including standing decaying waves have been found [25]. Also for a straight pipe with a discrete mass, large vibration amplifications were found at the cut-on frequencies of higher order radial–axial modes [4]. Consequently, before the velocity method can be used with confidence, more research in this area has to be undertaken to find limits for the strain concentration at equipment mounted on pipes.

ACKNOWLEDGMENT

This work was financially supported by EPSRC, UK. The first authors three-year repose at the ISVR was assisted by grants from TFR, Sweden.

REFERENCES

1. M. El-Raheb and P. Wagner 1985 *Journal of the Acoustical Society of America* **78**, 738–746. Harmonic response of cylindrical and toroidal shells to an internal acoustic field. Part 1: theory.
2. A. Wang and R. J. Pinnington 1990 *Proceedings of the Institute of Acoustics* **12**, 477–484. An impedance approach to pipework analysis using the transmission matrix method.
3. C. de Jong 1994 *Ph.D. Thesis, Technische Universiteit Eindhoven*. Analysis of pulsations and vibrations in fluid-filled pipe systems.
4. S. Finnveden 1997 *Journal of Sound and Vibration* **199**, 125–154 Spectral finite element analysis of the vibration of straight fluid-filled pipes with flanges.
5. M. P. Norton and A. Pruiti 1991 *Applied Acoustics* **33**, 313–336. Universal prediction schemes for estimating flow-induced industrial pipeline noise and vibration.
6. S. Finnveden 1997 *Proceedings of the IUTAM Symposium on Statistical Energy Analysis, Southampton*. Statistical energy analysis of fluid-filled pipes. Dordrecht: Kluwer Academic Publishers (to be published).
7. F. V. Hunt 1960 *Journal of the Acoustical Society of America* **32**, 1123–1128. Stress and strain limits on the attainable velocity in mechanical vibration.
8. E. E. Ungar 1961 *Journal of the Acoustical Society of America* **33**, 633–639. Transmission of plate flexural waves through reinforcing beams; dynamic stress concentrations.
9. S. M. Stearn 1970 *Journal of Sound and Vibration* **12**, 85–97. Spatial variation of stress, strain and acceleration in structures subject to broad frequency band excitation.
10. S. M. Stearn 1971 *Journal of Sound and Vibration* **15**, 353–365. The concentration of dynamic stress in a plate at a sharp change of section.
11. M. P. Norton and F. J. Fahy 1988 *Noise Control Engineering Journal* **30**, 107–117. Experiments on the correlation of dynamic stress and strain with pipe wall vibrations for statistical energy analysis applications.
12. L. L. Koss and D. Karzub 1995 *Journal of Sound and Vibration* **184**, 229–244. Euler beam bending wave solution predictions of dynamic strain using frequency response functions.

13. D. KARZUB 1996 *Ph.D. Thesis, The University of Western Australia*. The prediction of dynamic stress and strain in randomly vibrating structures using velocity measurements.
14. D. KARZUB and M. P. NORTON 1997 *Proceedings of the IUTAM Symposium on Statistical Energy Analysis, Southampton*. The estimation of dynamic stress and strain in beams, plates and shells using strain-velocity relationships. Dordrecht: Kluwer Academic Publishers (to be published).
15. N. W. M. BISHOP and F. SHERRAT 1989 *Environmental Engineering* **2**, 11–14, 29. Fatigue life prediction from power spectral density data. Part 1: traditional approaches.
16. A. W. LEISSA 1973 *NASA SP*-288. Washington, DC: U.S. Govt. Printing Office. Vibrations of shells.
17. R. N. ARNOLD and G. B. WARBURTON 1949 *Proceedings of the Royal Society of London, Series A* **197**, 238–256. Flexural vibrations of the walls of thin cylindrical shells having freely supported ends.
18. Y. C. FUNG 1965 *Foundations of Solid Mechanics*. Englewood Cliffs, NJ: Prentice-Hall.
19. S. FINNVEDEN 1997 *Journal of Sound and Vibration* **208**, 685–703. Simplified equations of motion for the radial–axial vibrations of fluid filled pipes.
20. R. S. LANGLEY 1994 *Journal of Sound and Vibration* **169**, 29–42. Wave motion and energy flow in cylindrical shells.
21. R. D. BLEVINS 1979 *Formulas for Natural Frequencies and Mode Shapes*. New York: Van Nostrand Reinhold Company.
22. S. H. LIU and R. J. PINNINGTON 1996 *Proceedings of Inter Noise*, 2773–2776. Measurement of flexural and longitudinal wave power flow in beams with piezoelectric films.
23. S. H. LIU 1996 *Ph.D. Thesis, University of Southampton*.
24. S. FINNVEDEN 1997 *Journal of Sound and Vibration* **208**, 705–728. Formulas for modal density and for input power from mechanical and fluid point-sources in fluid-filled pipes.
25. S. FINNVEDEN 1997 *Proceedings of the 6th International Conference on Recent Advances in Structural Dynamics, Southampton*, 613–627. Vibration energy transmission in fluid-filled pipes connected with flanges.